UNIVERSITY OF CALIFORNIA SAN DIEGO

Understanding the Structure and Function of Rhomboid Proteins

A Thesis submitted in partial satisfaction of the
requirements for the degree Master of Science

in

Chemistry

by

Anahita Nejatfard

Committee in charge:

Professor Sonya E. Neal, Chair
Professor Brian Zid, Co-Chair
Professor Andrew Kummel

2021

The Thesis of Anahita Nejatfard is approved, and it is acceptable in quality and form for publication on microfilm and electronically:

University of California San Diego

2021

Dedication

I would like to dedicate this thesis to my family, for always supporting me. I would also like to thank all members of the Neal Lab for their support and encouragement, and for making this lab feel like home these last years.

Epigraph

"You'd be amazed how much research you can get
done when you have no life whatsoever."

Ernest Cline

TABLE OF CONTENTS

List of Figures and Tables

Abbreviations

CHX	Cycloheximide
DDM	*n*-dodecyl-β-D-maltoside
Dfm1	DER1-like Family Member Protein 1
ERAD	Endoplasmic Reticulum-Associated Degradation
GAPDH	Glyceraldehyde-3-Phosphate Dehydrogenase
GFP	Green Fluorescent Protein
HA	Hemagglutinin
HMG2	3-Hydroxy-3-Methylglutaryl-Coenzyme A Reductase 2
Hrd1	HMG-CoA Reductase Degradation Protein 1
LB	Luria Broth
PCR	Polymerase Chain Reaction
Pdr5	Pleiotropic ABC Efflux Transporter of Multiple Drugs
RHBDL	Rhomboid Like
RING	Really Interesting New Gene
SC	Synthetic Complete
SDS-PAGE	Sodium Dodecyl Sulphate-Polyacrylamide Gel Electrophoresis
SMALPs	Styrene-Maleic Acid Lipid Particles
SPOCK	Single Plate Orf Compendium Kit
Ste6	Alpha-Factor-Transporting ATPase
SUS	Self-Ubiquitinating Substrate
Vma12	(/VPH2) Vacuolar ATPase Assembly Integral Membrane Protein

WT	Wildtype
YPD	Yeast-Peptone-Dextrose

Acknowledgements

I would like to acknowledge Sonya E. Neal, Ph.D. for endless amounts of guidance, encouragement, and support throughout my time in the Neal Lab.

I would also like to thank my committee members, Brian M. Zid, Ph.D., and Andrew Kummel, Ph.D. for their support and interest in my research.

Chapter 1, in full, is a reprint of the material as it appears in iScience 2020. Neal, Sonya E; Nejatfard, Anahita, CellPress 2020. The thesis author was the third author on this paper.

Chapter 2, in full, has been submitted for publication of the material as it may appear in Molecular Cell, 2021. Nejatfard, Anahita; Neal, Sonya E; Wauer, Nicholas; Amaro, Rommie E. The thesis author was the primary author of this paper.

ABSTRACT OF THE THESIS

Understanding the Structure and Function of Rhomboid Proteins

by

Anahita Nejatfard

Master of Science in Chemistry

University of California San Diego, 2021

Professor Sonya E. Neal, Chair

Professor Brian Zid, Co-Chair

ER-associated degradation (ERAD) targets misfolded ER proteins for degradation. Retrotranslocation, a key feature of ERAD, entails removal of ubiquitinated substrates into the cytosol for proteasomal destruction. Recent work in *S. cerevisiae* has revealed derlin rhomboid pseudoprotease Dfm1, related to the rhomboid superfamily, is involved in the retrotranslocation of ubiquitinated ERAD membrane substrates. Those studies also revealed a second, Hrd1-dependent pathway of ERAD-M retrotranslocation can arise in *dfm1*Δ null. In Chapter 1, we show the HRD complex undergoes remodeling to a form that mediates ERAD-M

retrotranslocation in the *dfm1*Δ null. Specifically, we found neither Hrd1 autoubiquitination nor its cytosolic domain is required for suppressive ERAD-M retrotranslocation. Thus, the HRD complex displays remarkable functional flexibility in response to ER stress. In Chapter 2, we found that Dfm1's conserved rhomboid residues are critical for membrane protein retrotranslocation. Specifically, we identified several retrotranslocation-deficient Dfm1 Loop1 mutants that display impaired binding to membrane substrates as well as TM2 mutants that retain lipid thinning functions of its rhomboid protease predecessors to facilitate in the removal of ER membrane substrates. This work reveals that derlin rhomboid pseudoproteases employ novel mechanisms of substrate engagement and lipid thinning for extracting multi-spanning membrane substrates. In Chapter 3, we sought to translate our studies of conserved rhomboid residues to mammalian rhomboid proteases by understanding preferential substrate specificity for rhomboid proteins RHBDL1 and RHBDL3. While the studies in this chapter were halted due to the pandemic, our studies provide valuable insight on the process of solubilizing and purifying these mammalian membrane proteins.

Introduction

Relevance of Protein Quality Control

Proteins play a fundamental role across all walks of life. They play critical roles in nearly every cellular process, including but not limited to cellular repair, the building of bones and bodily tissues, and assisting in metabolic reactions and immune responses.

In eukaryotes, nearly one third of the proteome is synthesized at the Endoplasmic Reticulum (ER) (1). These translated proteins enter the ER in an unfolded state, and the secretory pathway assists in the folding of these polypeptides into their tertiary and quaternary structures and trafficking to their final cellular destination. Proper folding of proteins, unique to their respective amino acid makeup, enables the protein to then be packaged and distributed off to various cells and tissues to execute a majority of cellular and organismal functions. As such, there is significant investment of cellular resources dedicated to the delicate task of protein folding.

Unfortunately, protein misfolding is inherently common, with 12-15% of newly synthesized proteins in human cells and 1-5% of newly synthesized proteins in yeast cells folding improperly (1). Often, this misfolding arises from either damage to the newly synthesized protein via chemical or UV damage, or from imbalanced subunit synthesis or genetic mutation (2). The accumulation of these misfolded proteins, if not eliminated, can lead to significant problems and cellular stress, underlying many human diseases including aging, cancer, and neurodegenerative disorders (2, 25, 26). To remedy the problem of protein misfolding and maintain cellular homeostasis, organisms are equipped with several quality control mechanisms enabling detection, rescue, and elimination of those aberrant proteins.

Endoplasmic Reticulum Associated Degradation

ER-Associated Degradation (ERAD) is an integral quality control process designed to eliminate improperly folded proteins (1). It is a highly conserved pathway that selectively targets misfolded proteins for degradation, preventing potential maladies that can arise (3). Defective ERAD can result in the buildup of those damaged and disease-causing proteins. Additionally, ERAD machinery can be manipulated by pathogens and in cancer progression, bringing relevance to its study (4-5).

ERAD involves several key steps: 1) recognition of misfolded protein substrates, 2) polyubiquitination of those substrates using ER resident ubiquitin E3 ligases, 3) transfer of those ubiquitinated substrates to the cytosol, a process powered by Cdc48/p97 AAA-ATPase and known as retrotranslocation, and 4) degradation by the cytosolic proteasome (6-7). Work in the budding yeast, *S. cerevisiae*, revealed misfolded proteins are recognized and ubiquitinated either through ERAD of substrates with misfolded lesions within the ER lumen (ERAD-L), of substrates with misfolded lesions in the cytosolic domain (ERAD-C), or of integral membrane substrates with lesions in their transmembrane domain (ERAD-M) (8) (Figure 1).

In *S. cerevisiae,* the HRD pathway is an ERAD pathway, comprised of the E3 ligase Hrd1, which recognizes and ubiquitinates both ERAD-M and ERAD-L substrates, as well as some normal proteins such as the Hmg2 isoenzyme of HMG-CoA reductase (9). The DOA pathway, meanwhile, involves the E3 ligase Doa10, which recognizes and ubiquitinates ERAD-C substrates (9).

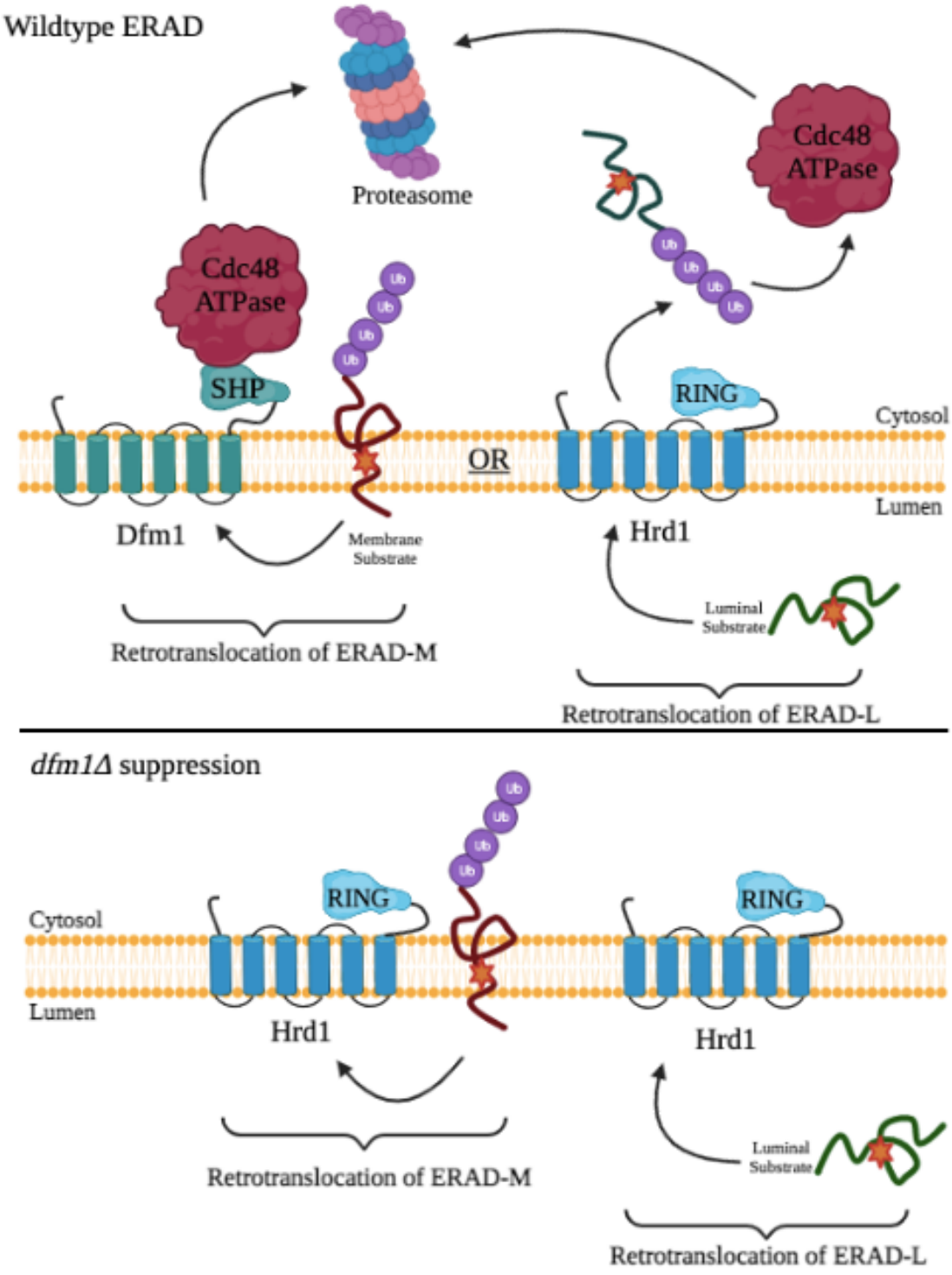

Figure 1. Wildtype ERAD and Proposed *dfm1*Δ Suppression Mechanism

Common to all ERAD pathways is the need to transfer misfolded substrates from the ER to the cytosol for proteasomal degradation, a process termed retrotranslocation or dislocation (10). This process requires an energy source for substrate removal, provided by the Cdc48 ATPase in yeast (p97 in mammals). The high degree of conservation regarding retrotranslocation has yielded an intense need to study the mechanism(s) that may be at play during this process.

Recent studies have revealed that multi-spanning E3 ligases Doa10 and Hrd1 serves as retrotranslocons for ERAD-L substrates, with Hrd1 serving as a retrotranslocation channel for ERAD-L substrates (12, 13). The identity of an analogous channel for ERAD-M substrates remained unclear until only recently. Garza et al. demonstrated Hrd1 is dispensable for the full retrotranslocation of a self-ubiquitinating substrate (SUS), presenting the idea that ERAD-M substrates potentially utilize a Hrd1-independent route out of the ER membrane (14). SUS-GFP is comprised of Hrd1's catalytic RING bound to Hmg1 among other units, which enables SUS-GFP to undergo autoubiquitination outside of Hrd1. This provides a powerful tool for uncoupling Hrd1's ubiquitination function from its potential retrotranslocation function. Prompted by this, Neal et al. employed SUS-GFP to screen the complete collection of yeast mutants with the Single Plate Orf Compendium Kit (SPOCK) array, consisting of a 5,808 yeast strain array of non-essential gene deletion mutants and essential DAmP gene mutants. This work led to identification of Dfm1 as an independent and dedicated mediator for retrotranslocating ERAD-M substrates, including those from both the HRD and DOA pathways as well as Hrd1 itself in circumstances where it is rapidly degraded by self-ubiquitination (11). The mechanisms behind Dfm1's role in ERAD-M and how it works in both the DOA and HRD pathways remains unclear, signifying importance in its study.

The Rhomboid Superfamily

Rhomboid proteins are integral membrane proteins that are perhaps one of the most widely conserved protein families known and play a role in many diverse membrane-related processes (16). Recent advances have highlighted the rhomboid superfamily of proteins to be involved in protein quality control pathways, including ERAD (15). Rhomboid proteins share a novel intramembrane serine protease activity that allows them to cleave substrate proteins in or near their transmembrane domains within the lipid bilayer, subsequently releasing them from the membrane into the luminal or extracellular environments. A subclass of rhomboids has evolved to lack those catalytic residues their protease predecessors have; they are termed rhomboid pseudoproteases (2). Despite the lack of protease activity, these pseudoproteases are just as biologically relevant, operating in trafficking of proteins, regulation of sterols, lipid homeostasis, and in signaling pathways (17).

Derlins are a subclass of the rhomboid family that have been discovered to be key mediators of ER protein quality control in yeast and mammals (2). Sequence and structural homology have revealed them to share structural similarities to rhomboids. Specifically, they are ER-resident integral membrane proteins and predicted to have transmembrane helices that span the lipid bilayer six times (18). Derlins have also emerged as those likely responsible for the retrotranslocation of substrates in ERAD, with yeast Der1 shown to possess membrane perturbation properties that assist in the retrotranslocation of ERAD-L substrates alongside Hrd1 (20). Yeast Dfm1 which as Neal et al. uncovered, acts as a mediator in retrotranslocating ERAD-M substrates also belongs to the derlin rhomboid family.

Derlins Dfm1 as well as human Derlin-1, found to play a role in assisting a viral component, US11, in degrading class 1 MHC heavy chain (MHC-1) within an infected host,

were shown to contain a unique, conserved sequence aiding in their role (19). They possess a unique C-terminal SHP box enabling their direct recruitment of Cdc48/p97 ATPase to the ER membrane, essential to the retrotranslocation process (11). This contradicted previous data suggesting Dfm1 played no role in ERAD, however this was discovered to be false: instead, the rapid rise of suppressive machinery in *dfm1*Δ null strains effectively masked the effect dfm1's absence had on retrotranslocation (11). Derlins like Dfm1 and human Derlin-1 lack proteolytic activity, yet their sequences indicate preservation of conserved rhomboid residues, perhaps signifying an overlap in their functions (11).

In general, rhomboid proteases possess a unique ability to cleave their membrane anchored substrates at specific sites within the lipid bilayer, a process mediated through their conserved serine-histidine dyad at the active site (2). Further studies surrounding rhomboid proteases indicate they can recognize structurally unstable features across transmembrane and extramembrane domains of a protein (23). For example, mammalian rhomboid RHBDL4 (also known as Rhbdd1) was shown to cleave multiple membrane proteins in their ectodomains, including amyloid precursor protein (APP), the incorrect cleavage of which can result in amyloid B (AB) peptides implicated in Alzheimer's disease (21). Other studies have noted rhomboids for their compact fold and small hydrophobic thickness, theorizing an ability to both diffuse quickly in the membrane as well as induce deformation of the local lipid bilayer (24).

Knowledge of how membrane-embedded rhomboid proteins interact with the lipid bilayer is important for beginning to understand how they interact with substrates and how the composition of the lipid membrane could influence their catalysis. In support of this idea, molecular dynamics of wild-type and mutant bacterial rhomboid protease GlpG in different membrane environments was analyzed (22). The GlpG protein displayed an irregular shape and

small hydrophobic thickness, both of which caused significant bilayer deformations. This information, coupled with the effects of region-specific mutations that drastically reduced the activity of the catalytic site, led to the presumption that GlpG's deformational thinning of the lipid bilayer may be important for substrate access prior to cleavage (22).

The conserved rhomboid residues in derlins suggests that they may also exhibit these functions in their role in the retrotranslocation process. Recent work has revealed that indeed to be true: using cryo-electron microscopy, the Rapaport lab published that Dfm1's paralog, a yeast derlin known as Der1, possesses hydrophilic residues with membrane perturbation properties (20). This induction of lipid thinning alongside E3 ligase Hrd1 allows for its ability to retrotranslocate ERAD-L substrates (20). However, whether the same mechanism of lipid thinning can be applied to the removal of integral membrane proteins from the ER has yet to be determined. An intriguing possibility is that Dfm1 has also retained these membrane perturbing properties that allow it to facilitate the movement of substrates across the membrane. These important discoveries and ideas solicit further research into the structure-function studies of both rhomboids and derlins.

Chapter 1: Hrd1's Ubiquitination Function is Dispensable for the Suppressive Pathway

Amplified Hrd1 Levels Sufficient for Suppressing dfm1Δ cells

Neal et al. identified derlin Dfm1 to play a role as a mediator in the retrotranslocation of ERAD-M substrates (11). This was initially perplexing due to previous reports showing Dfm1 had a lack of involvement in either HRD or DOA-dependent ERAD (40, 41). They were able to resolve these discrepancies by showing *dfm1*Δ strains undergo rapid suppression when exhibiting strong expression of ERAD-M substrates, such as Hmg2-GFP from the HRD pathway (Figure 2B-D). To test for suppression, a culture of the bright *dfm1*Δ + SUS-GFP starting strain (P0) was repeatedly passaged into fresh minimal medium followed by growth to saturation. By the fourth passage (P4), approximately half of the cells were comparable to the dark cells in the wild type while the other half remained bright. By P11, the culture population was entirely composed of dark cells, with a histogram identical to that of the wild-type strain (Figure 2A). In those null strains, retrotranslocation and degradation of ERAD-M substrates were completely restored, characterizing a potential alternative stress pathway for ERAD-M substrate removal (Figure 2E-F).

Neal et al. found the E3 ligase Hrd1, typically involved in ERAD-L, was required for suppression of *dfm1*Δ nulls, with a *dfm1*Δ*hrd1*Δ null resulting in no suppression and masked phenotype (Figure 3A-C). They determined this by developing an "instant suppression assay" in which the Hrd1 plasmid is transformed into *dfm1*Δ*hrd1*Δ cells strongly expressing SUS-GFP. If Hrd1 was sufficient to suppress the *dfm1*Δ deficiency, then those colonies with enough copies of the Hrd1-expressing plasmid would show the masked phenotype of SUS-GFP degradation. As expected, about ten percent of the total transformants displayed low colony fluorescence,

indicating restored SUS-GFP retrotranslocation and degradation. Suppressees were found to yield a duplicated yeast chromosome XV, where the gene for the HRD1 locus resides. Adding back Hrd1 to an autonomously maintained ARS/CEN plasmid resulted in the suppressive mechanism without chromosome duplication, signifying Hrd1 to be the relevant factor for said duplication (Figure 3D). This theory was affirmed when all the suppressees revealed approximately 5-fold levels of elevated Hrd1 expression compared to normal expression (Figure 3E). Altogether, this data implied Hrd1's essential role in the restorative alternative retrotranslocation pathway for ERAD-M in the absence of Dfm1.

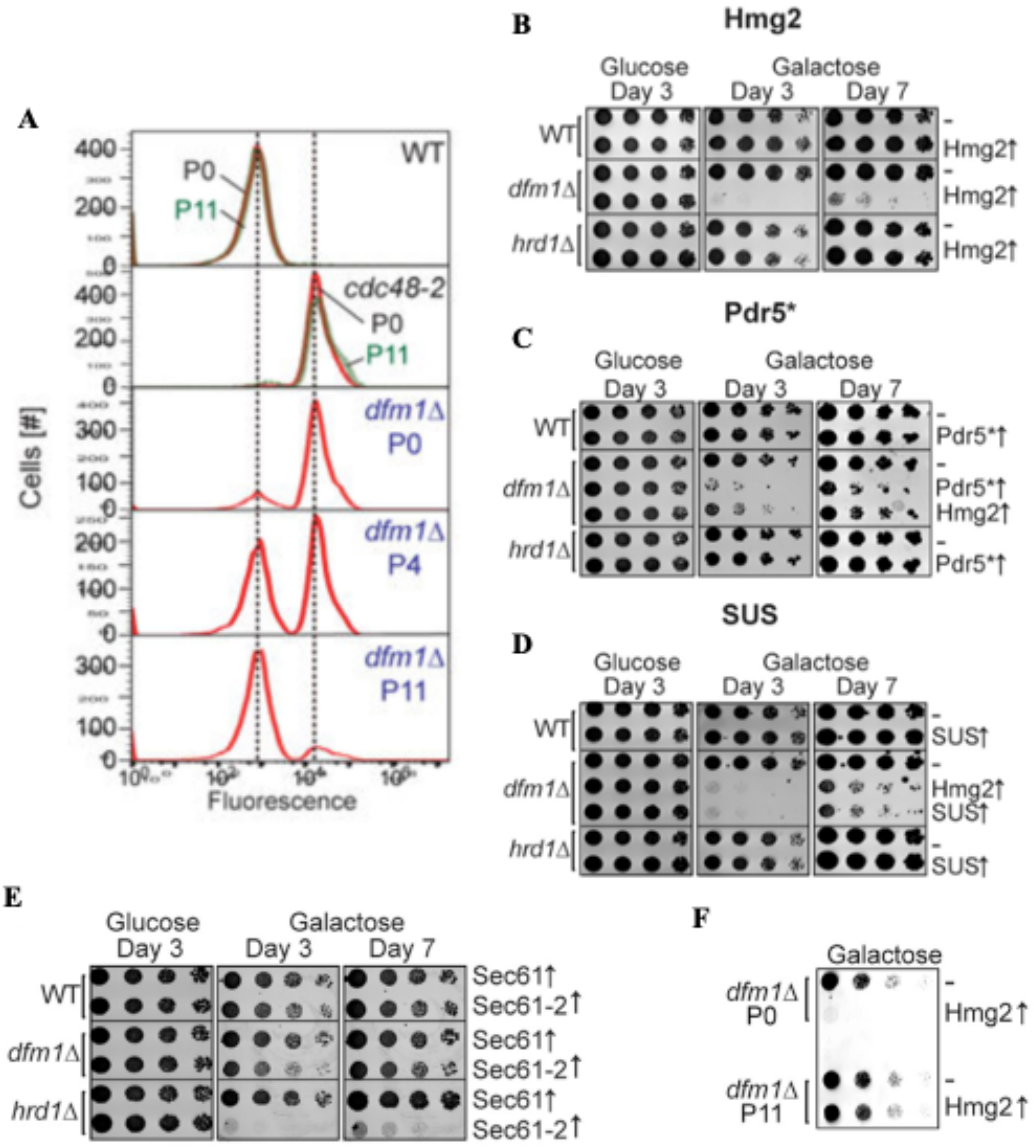

Figure 2. *Dfm1*Δ Cells with Strongly Expressed ERAD-M Substrates See Growth Defect Suppression
(A) *dfm1*Δ cells containing overexpressed SUS-GFP were passaged to suppression. The indicated cells with overexpressed SUS-GFP were passaged at the indicated number of times into fresh minimal media (P0, P4, and P11) and SUS-GFP levels were analyzed by flow cytometry. Histograms of 10,000 cells are show, with the number of cells versus GFP fluorescence. Panels are aligned so all fluorescent histograms are comparable between panels. (B) Galactose-induced Hmg2-GFP overexpression causes a growth defect in *dfm1*Δ cells. WT, *dfm1*Δ, and *hrd1*Δ cells containing empty vector or GAL-driven Hmg2-GFP were compared for growth by dilution assay. Each strain was spotted in 5-fold dilutions on glucose or galactose-containing plates to drive Hmg2-GFP overexpression. Plates were incubated at 30°C. (C-D) WT, *dfm1*Δ, and *hrd1*Δ cells were spotted in 5-fold dilutions on glucose or galactose-containing plates to drive overexpression of Pdr5*-HA and SUS-GFP. (E-F) Same as (B) except non-passaged *dfm1*Δ and *dfm1*Δ*hrd1*Δ non-passaged cells (P0) or cells passaged to suppression (P11) were assessed for growth defect in the dilution assay.

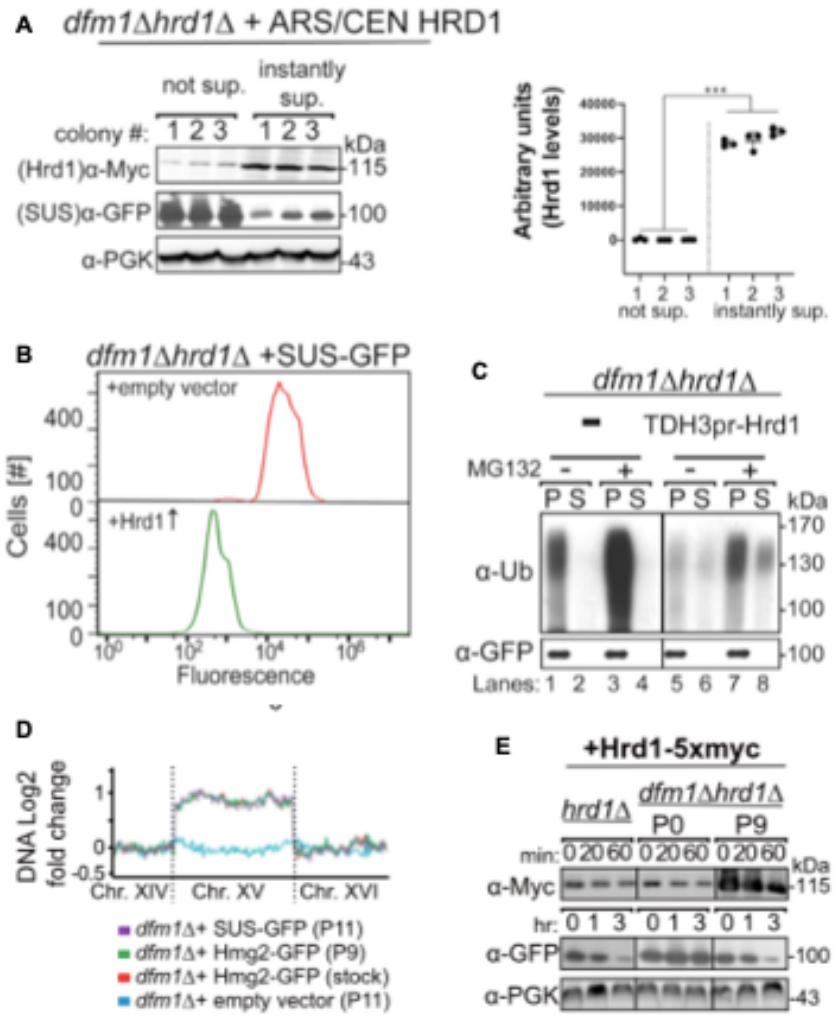

Figure 3. Elevated Hrd1 Levels Essential to *Dfm1*Δ-Mediated Suppression
(A) Increased Hrd1 copy number instantly suppressed *dfm1*Δ*hrd1*Δ cells. *dfm1*Δ*hrd1*Δ cells overexpressing SUS-GFP were transformed with an ARS/CEN Hrd1 plasmid. Subsequently, transformants were screened for instantly suppressed non-fluorescent dark colonies. Both non-suppressed (bright colonies; n=9) and suppressed cells (dark colonies; n=9) were grown to log phase, lysed, and analyzed by SDS-Page and immunoblotted for steady-state levels of Hrd1 with α-myc and SUS with α-GFP. Mean ± SEM, ***p < 0.001, nested t test. (B) Strongly expressed Hrd1 instantly suppresses *dfm1*Δ*hrd1*Δ + SUS-GFP cells. *dfm1*Δ*hrd1*Δ + SUS-GFP cells were transformed with empty vector or TDH3pr-Hrd1. SUS-GFP levels were analyzed by flow cytometry. Histograms of 10,000 cells are shown, with the number of cells versus GFP fluorescence. Panels are aligned so all fluorescent histograms are comparable between panels. (C) *in vivo* SUS-GFP retrotranslocation is restored in instantly suppressed *dfm1*Δ*hrd1*Δ cells. Crude lysate was prepared from the indicated strains treated with vehicle or MG132 (25 ug/mL). Lysates were ultracentrifuged to discern ubiquitinated SUS-GFP that either has been retrotranslcoated into the soluble fraction (S) or remained in the membrane (P). Following fractionation, SUS-GFP was immunoprecipitated from both fractions, resolved on 8% SDS-PAGE, and immunoblotted with α-GFP or α-Ubi. (D) ChrXV duplication is substrate induced upon loss of Dfm1. Chromosome profiles of whole genome sequencing data mapped across ChrXV. Genomic levels through entire ChrXV are twice as high in suppressed *dfm1*Δ cells expressing Hmg2-GFP or SUS-GFP with respect to those expressing empty vector. (E) Hrd1 levels are upregulated in *dfm1*Δ suppressees. Degradation of Hrd1-5xmyc was measured by CHX-assay in *dfm1*Δ P0 and d*fm1*Δ P11 overexpressing Hmg2-GFP. After CHX, cells were lysed at indicated times, analyzed by SDS-PAGE, and immunoblotted for Hrd1 with α-Myc and Hmg2 with α-GFP.

HRD Complex Components Not Required for Suppressive Retrotranslocation Pathway

Hrd1 functions as part of the HRD complex, composed of the Hrd1's cytoplasmic RING motif required for ubiquitination, the protein Usa1, with a cytoplasmic Ubiquitin-like (Ubl) domain, and the mostly luminal protein Hrd3 (Figure 4A). We reasoned that Hrd1 partner proteins were required for the suppressive retrotranslocation pathway. Under normal genomic levels, Hrd1 requires both Hrd3 and Usa1 for the HRD complex to perform its function. However, in the alternative pathway, Neal et al. found both proteins to be dispensable for Hrd1-mediated suppression (Figure 4B).

In fact, Hrd3 appeared to lack a presence in the suppressed cells, and with addition of proteasome inhibitor MG132, was found to undergo efficient proteasomal degradation (Figure 4C-D). Moreover, when Hrd3 was overexpressed in the suppressed *dfm1*Δ nulls, a drastic growth defect was observed, signifying an antagonistic role for Hrd3 in the Hrd1-mediated suppressive pathway (Figure 4E-F).

Figure 4. Hrd3 of HRD Complex Rapidly Degraded in Suppressive Pathway
(A) Depiction of the HRD complex comprised of E3 ligase Hrd1, its partner, Hrd3, and Usa1, which recognizes and ubiquitinates ERAD-M and ERAD-L substrates. (B) Hrd3 and Usa1 are dispensable for suppression. Indicated strains overexpressing SUS-GFP were passaged to suppression, with SUS-GFP levels analyzed by flow cytometry. Histograms of 10,000 cells are show, with number of cells versus GFP fluorescence. (C) Hrd3 is rapidly degraded in *dfm1*Δ suppressees. Steady-state levels of indicated proteins were analyzed in *dfm1*Δ P0 and *dfm1*Δ P11 cells strongly expressing Hmg2-GFP. Cells were lysed, analyzed by SDS-PAGE, and immunoblotted for Hrd1 with α-Myc, Hmg2 with α-GFP, α-Cdc48, and Hrd3 with α-HA. (D) Degradation of Hrd3 was measured by CHX-chase assay in passaged suppressed *dfm1*Δ P11 strains treated with vehicle or MG132 (25 μg/mL). After CHX addition, cells were lysed at indicated times, analyzed by SDS-PAGE, and immunoblotted for Hrd3 with α-HA. Band intensities were normalized to PGK1 loading control and quantified by ImageJ. t=0 was taken as 100% and data are represented as mean ± SEM from at least three experiments, ***$p < 0.001$, repeated measures ANOVA. (E) Galactose-induced Hrd3 overexpression causes cell lethality in *dfm1*Δ suppressed cells. WT, *hrd1*Δ, and *dfm1*Δ suppressed cells overexpressing Hmg2-GFP (left) or SUS-GFP (right) and harboring either empty vector or GAL-driven Hrd3 were compared for growth by dilution assay. Each strain was spotted in 5-fold dilutions on glucose or galactose-containing plates to drive Hrd3 overexpression. Plates were incubated at 30°C. (F) Hrd3 overexpression blocks restoration of ERAD-M retrotranslocation. WT and *dfm1*Δ cells overexpressing SUS-GFP were grown in the presence of glucose to turn of Hrd3 expression and passaged to suppression at the indicated number of times into fresh minimal media (P11). P11WT and *dfm1*Δ cells were then passaged into minimal media containing galactose as a sole carbon source to trigger Hrd3 overexpression (P12). Flow cytometry was used to assess SUS-GFP steady-state levels. Histograms of 10,000 cells are shown, with number of cells versus GFP fluorescence.

Hrd1's Ubiquitination Activity Regarding Suppressive ERAD-M

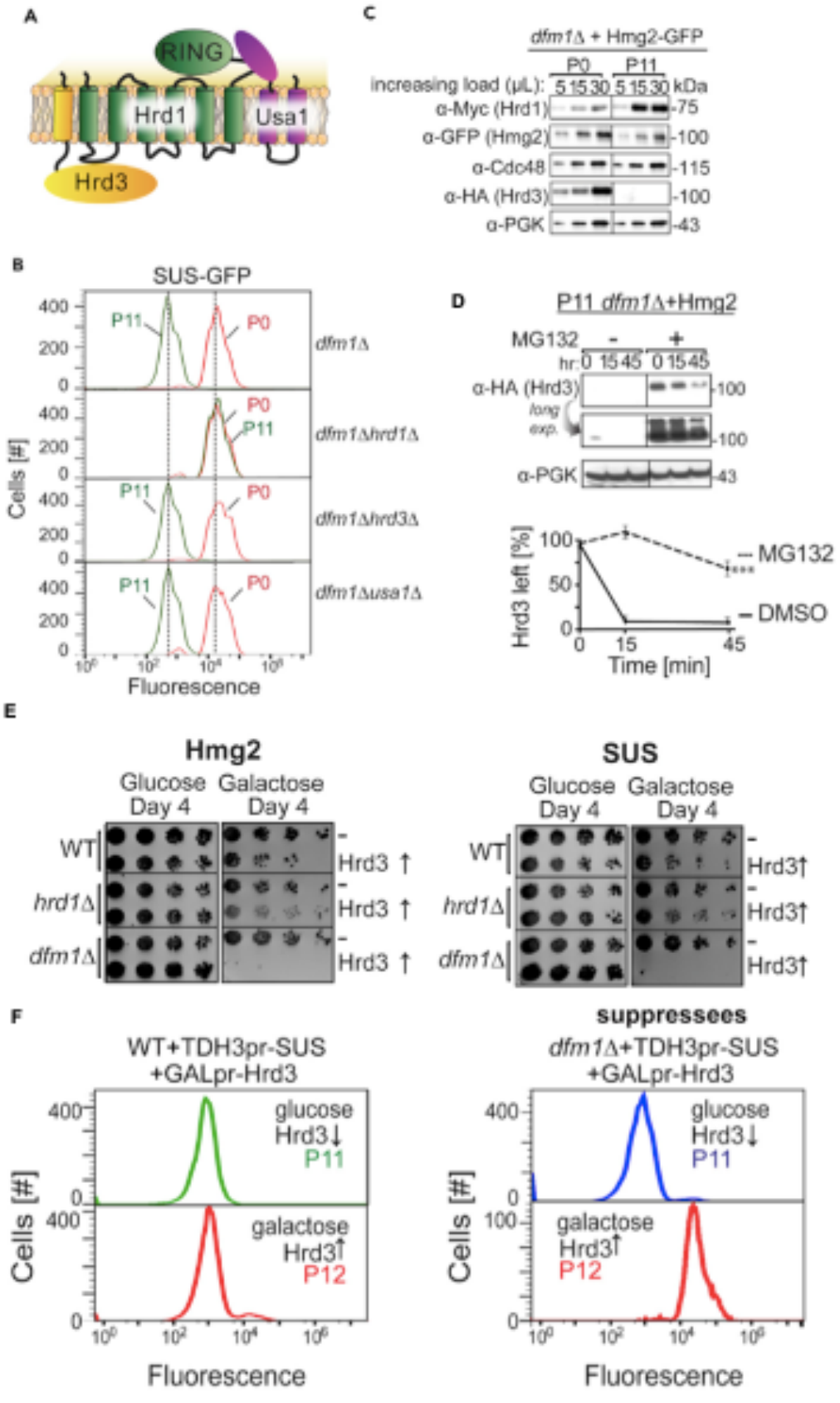
A
RING
Hrd1
Usa1
Hrd3
C
dfm1Δ + Hmg2-GFP
P0
P11
increasing load (µL): 5 15 30 5 15 30 kDa
α-Myc (Hrd1)
α-GFP (Hmg2)
α-Cdc48
α-HA (Hrd3)
α-PGK
-75
-100
-115
-100
-43
B
SUS-GFP
P11
P0
dfm1Δ
dfm1Δhrd1Δ
dfm1Δhrd3Δ
dfm1Δusa1Δ
Cells [#]
Fluorescence
D
P11 dfm1Δ+Hmg2
MG132 - +
hr: 0 15 45 0 15 45
α-HA (Hrd3)
long exp.
α-PGK
-100
-100
-43
Hrd3 left [%]
MG132
DMSO
Time [min]
E
Hmg2
SUS
Glucose Day 4
Galactose Day 4
WT
hrd1Δ
dfm1Δ
Hrd3 ↑
Hrd3↑
F
WT+TDH3pr-SUS +GALpr-Hrd3
dfm1Δ+TDH3pr-SUS +GALpr-Hrd3
suppressees
glucose
Hrd3↓
P11
galactose
Hrd3↑
P12
Cells [#]
Fluorescence

Neal et al. reported that Hrd1's ubiquitination activity was not a requirement for its role in the *dfm1*Δ suppressive pathway for ERAD-M substrates (11). This was a surprise, given that Baldridge et al. previously reported that autoubiquitination of Hrd1 on several lysines of its RING-finger domain is essential in ERAD-L, allowing the misfolded luminal domain of a substrate to move across the membrane (13). However, upon further examination of Hrd1 mutants CS339, inactive in its ubiquitination function, and hemi-Hrd1, a truncated version of Hrd1 with its transmembrane domain intact but its catalytic RING domain removed (Figure 5A), their results demonstrated quite the opposite for this suppressive pathway. Initially, *dfm1*Δ strains expressing Hrd1, C399S-Hrd1, and hemi-Hrd1 under control of the strong TDH3 promoter failed to restore retrotranslocation of SUS-GFP when Hrd3 was not removed (Figure 5B). Removing Hrd3 and its potentially antagonistic role, however, enabled the C399S-Hrd1 mutant to recover the suppressees (Figure 5B). To further test this idea, hemi-Hrd1 was also able to fully restore substrate degradation when Hrd3 was removed (Figure 5C). With normal retrotranslocation of substrate seen, these results confirm ERAD-M retrotranslocation does not require Hrd1's ubiquitination activity. They also present the idea that Hrd1's ubiquitination function is necessary not for restoration of retrotranslocation in this suppressive pathway, but instead assists in the removal of toxic Hrd3.

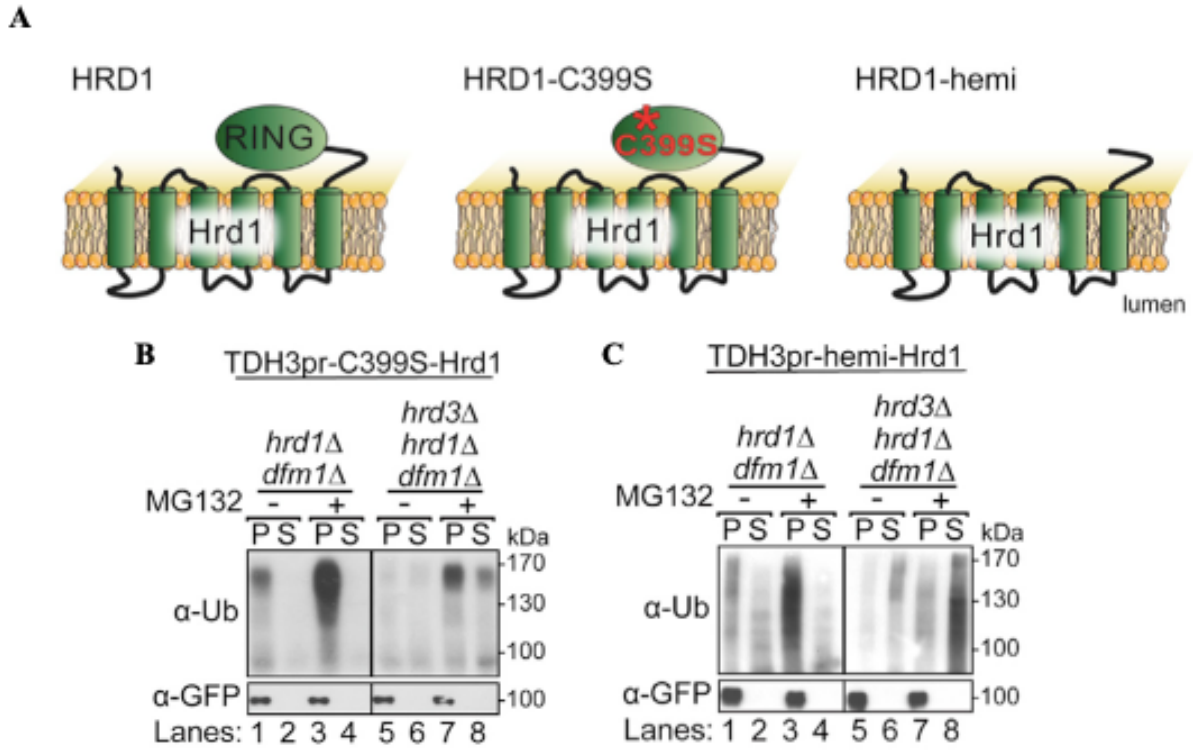

Figure 5. Hrd1's Ubiquitination Activity is Dispensable for Suppressive ERAD-M Retrotranslocation
(A) Depiction of E3 ligase Hrd1, C399S-Hrd1, and hemi-Hrd1. C399S-Hrd1 is an inactive version of Hrd1 where the essential cysteine is mutated in the RING finger. Hemi-Hrd1 is a truncated version of Hrd1 containing only the transmembrane domain. (B) Overexpression of C399S-Hrd1 is sufficient for retrotranslocation of SUS-GFP in *dfm1*Δ*hrd1*Δ*hrd3*Δ cells. Crude lysate was prepared from the indicated strains treated with vehicle or MG132 (25 μg/mL). Lysates were ultracentrifuged to discern ubiquitinated SUS-GFP that either has been retrotranslocated into the soluble fractions (S) or remained in the membrane (P). Following fractionation, SUS-GFP was immunoprecipitated from both fractions, resolved on 8% SDS-PAGE, and immunoblotted with α-GFP and α-Ubi. (C) Same as (B) except with strongly expressed hemi-Hrd1 (or *dfm1*Δ*hrd1*Δ*hrd3*Δ cells with empty vector), with hemi-Hrd1 sufficient for restoring retrotranslocation of SUS-GFP.

To summarize, Neal et al. discovered the *dfm1*Δ null phenotype is rapidly suppressed when expressed alongside strong levels of ERAD-M substrates. Through their instant suppression assay, they found adding Hrd1 back to *dfm1*Δ*hrd1*Δ double null strains leads to restoration of the retrotranslocation and degradation of those ERAD-M substrates, characterizing an alternative pathway for removing integral membrane substrates. Suppressed strains yielded a duplicated yeast chromosome XV, where the gene for the Hrd1 locus resides and ultimately was affirmed to be the relevant factor behind the duplication. Thus, Hrd1 acts as a mediator of this

*dfm1*Δ-suppressive retrotranslocation. Other components of the HRD complex, proteins Usa1 and Hrd3, were found to be dispensable for this Hrd1-mediated suppression. Furthermore, Hrd3 appeared to play an antagonistic role, causing a drastic growth defect when overexpressed in the suppressed *dfm1*Δ strains**.** Lastly, Hrd1 utilizes its catalytic RING domain in ERAD-L to ubiquitinate luminal substrates for degradation; however, in this alternative ERAD-M pathway, Hrd1's ubiquitination activity appears to be unnecessary for the retrotranslocation of membrane substrates, instead assisting in the removal of toxic Hrd3.

Study Aims and Goals

Our goal is to demonstrate that Hrd1's ubiquitination activity is truly dispensable despite unintentional reinstatement of active Hrd1. The experiments above used a bona-fide substrate, SUS-GFP. Despite the results mentioned above, the use of SUS-GFP as the substrate in these experiments cannot fully support the conclusion that Hrd1's ubiquitination activity is dispensable for the suppressive retrotranslocation pathway. For instance, Gardner et al. previously showed co-expression of hemi-Hrd1 and RING-Hrd1 (containing only its RING domain) restored Hrd1 function in the *hrd1*Δ null strain (26). Similarly, the use of SUS-GFP, whose structure retains Hrd1's catalytic RING domain to enable its rapid and independent self-ubiquitination, enables the possibility for the C399S-Hrd1 and hemi-Hrd1 mutants to interact with its trans-expressed RING domain.

To address this issue, our goal is to use bona-fide substrates of the ERAD pathway that can bypass Hrd1's ubiquitination function; allowing us to discern for Hrd1's potential ubiquitin-independent function. To that end, we will utilize membrane substrates, Ste6* and Deg1-Vma12-GFP in our suppression experiments. Both are membrane substrates of the DOA pathway, which

relies on E3 ligase Doa10 for ubiquitination and degradation along with Dfm1 for retrotranslocation.

My hypothesis is that *dfm1*Δ-mediated restoration of DOA-dependent ERAD-M substrates does not require Hrd1's ubiquitination activity.

Materials and Methods

Yeast and Bacteria Growth Media

Standard yeast *Saccharomyces cerevisiae* growth media was used, including yeast extract-peptone-dextrose (YPD) medium and ammonia-based synthetic complete dextrose (SC) supplemented with 2% dextrose and amino acids to enable growth of auxotrophic strains at 30°C.

Plasmids and Strains

Plasmids used in this study are listed in Table 1. Plasmids for this work were generated using standard molecular biology cloning techniques via polymerase chain reaction (PCR) of genes from yeast genomic DNA or plasmid followed by ligation into a specific restricted digested site within a construct and verified by sequencing (Eton Bioscience, Inc.). A complete list of yeast strains and their corresponding genotypes are listed in Table 2. All strains used in this work were derived from S288C or Resgen. Yeast strains were transformed with DNA or PCR fragments using the standard LiOAc method in which null alleles were generated by using PCR to amplify a selection marker flanked by 50 base pairs of the 5' and 3' regions, which are immediately adjacent to the coding region of the gene to be deleted. The selectable markers used for making null alleles were genes encoding resistance to G418 or CloNAT/nourseothricin. After transformation, strains with drug markers were plated onto YPD followed by replica-plating onto YPD plates containing 500 μg/mL G418 or 200 μg/mL nourseothricin. All gene deletions were confirmed by PCR.

Table 1. List of Plasmids Used in this Thesis, Related to Figure 6

Plasmid	Plasmid Type	Yeast Marker	Gene
pRH2513	YIp	TRP1	pTDH3-HRD1-MYC
pRH2514	YIp	TRP1	pTDH3-HRD1-C399S-MYC
pRH1246	YIp	LEU2	pTDH3-HRD1-hemi-MYC
pRH2515	YIp	TRP1	pMET25-DEG1-FLAG-VMA12-GFP

Table 2. List of Yeast Strains Used in this Study, Related to Figure 6

Strain	Genotype
RHY 11064	Mata *ade2-101 met2 lys2-801 his3Δ200 trp1::hisG::TRP1::TDH3pr-HRD1-MYC leu2Δ ura3-52 dfm1Δ::NatR hrd1Δ::KanMX CEN::URA3::STE6-166-HA-GFP*
RHY 11076	Mata *ade2-101 met2 lys2-801 his3Δ200 trp1::hisG::TRP1::TDH3pr-C399S-HRD1-MYC leu2Δ ura3-52 dfm1Δ::NatR hrd1Δ::KanMX CEN::URA3::STE6-166-HA-GFP*
RHY 11077	Mata *ade2-101 met2 lys2-801 his3Δ200 trp1::hisG::TRP1::TDH3pr-hemi-HRD1-MYC leu2Δ ura3-52 dfm1Δ::NatR hrd1Δ::KanMX CEN::URA3::STE6-166-HA-GFP*
RHY 11112	Mata *ade2-101 met2 lys2-801 his3Δ200 trp1::hisG::TRP1::TDH3pr-C399S-HRD1-MYC leu2Δ ura3-52 dfm1Δ::NatR hrd1Δ::KanMX CEN::URA3::STE6-166-HA-GFP hrd3Δ::LEU2*
RHY 10890	Mata *ade2-101 met2 lys2-801 his3Δ200 trp1::hisG::TRP1::MET25pr-Deg1-FLAG-VMA12-GFP leu2Δ ura3-52::URA3::TDH3pr-HRD1-MYC dfm1Δ::NatR hrd1Δ::KanMX*
RHY 10891	Mata *ade2-101 met2 lys2-801 his3Δ200 trp1::hisG::TRP1::MET25pr-Deg1-FLAG-VMA12-GFP leu2Δ ura3-52::URA3::TDH3pr-C399S-HRD1-MYC dfm1Δ::NatR hrd1Δ::KanMX*
RHY 10892	Mata *ade2-101 met2 lys2-801 his3Δ200 trp1::hisG::TRP1::MET25pr-Deg1-FLAG-VMA12-GFP leu2Δ ura3-52::URA3::TDH3pr-hemi-HRD1-MYC dfm1Δ::NatR hrd1Δ::KanMX*
RHY 10893	Mata *ade2-101 met2 lys2-801 his3Δ200 trp1::hisG::TRP1::MET25pr-Deg1-FLAG-VMA12-GFP leu2Δ ura3-52::URA3::TDH3pr-C399S-HRD1-MYC dfm1Δ::NatR hrd1Δ::KanMX hrd3Δ::LEU2*
RHY 10894	Mata *ade2-101 met2 lys2-801 his3Δ200 trp1::hisG::TRP1::MET25pr-Deg1-FLAG-VMA12-GFP leu2Δ ura3-52::URA3::TDH3pr-hemi-HRD1-MYC dfm1Δ::NatR hrd1Δ::KanMX hrd3Δ::LEU2*
RHY 10907	Mata *ade2-101 met2 lys2-801 his3Δ200 trp1::hisG::TRP1::TDH3pr-hemi-HRD1-MYC leu2Δ ura3-52 dfm1Δ::NatR hrd1Δ::KanMX CEN::URA3::STE6-166-HA-GFP hrd3Δ::LEU2*

dfm1Δ Strain Handling

To observe the phenotypic effect of *dfm1Δ* null strains, freshly transformed *dfm1Δ* null cells with the respective ERAD-M substrates was used in every assay.

Cell Passaging

To observe suppression, *dfm1Δ* null strains with strongly expressed SUS-GFP were inoculated in fresh minimal selection media (-Ura). Once cells are grown to stationary phase, cells were passaged into fresh minimal selection media (.05 ODs) and grown to stationary phase. Cells were repeatedly passaged this way until *dfm1Δ* null strains are suppressed (typically by 8-10 passages).

Cycloheximide-Chase Assay

Cycloheximide chase assays were performed in which cells were grown to log-phase (OD_{600} 0.2-0.3) and cycloheximide was added to a final concentration of 50 μg/mL. At each time point, a constant volume of culture was removed and lysed. Lysis was initiated with addition of 100 μL SUME with protease inhibitors (PIs) and glass beads, followed by vortexing for 4 minutes. 100 μL of 2xUSB was added followed by incubation at 55°C for 10 minutes. Samples were clarified by centrifugation and analyzed by SDS-PAGE and Immunoblotting.

Microsome Isolation

Yeast strains were grown to log phase (OD_{600} 0.2-0.3) and 15 ODs of cells were pelleted. Cells were resuspended in H_2O, centrifuged, and lysed with the addition of 0.5 mM glass beads and 400 μL of MF buffer with PIs and vortexed in 1-minute intervals on and off for 12 minutes

at 4°C. Lysates were combined and clarified by centrifugation at 1,500 x g for 5 minutes at 4°C. Supernatant was transferred to another tube and centrifuged at 14,000 x g for 1 minute at 4°C. 60 µL of 2xUSB was added to microsome fractions followed by solubilization at 55°C for 10 minutes. Samples were clarified by centrifugation, analyzed by SDS-PAGE, and immunoblotted.

Results

*Hrd1's Ubiquitination Function is Dispensable for Retrotranslocating DOA Substrate, Ste6**

Since the trans-expressed RING domain on SUS-GFP could potentially interact with Hrd1 derivatives, we turned our attention to using canonical ERAD membrane substrate, Ste6*. To test whether this DOA substrate can be degraded in the Hrd1-mediated suppressive pathway, cycloheximide-chase assays were performed on *dfm1*Δ*hrd1*Δ strains expressing either wild-type (WT) Hrd1, inactive C399S-Hrd1, or hemi-Hrd1 driven by a strong TDH3 promoter alongside Ste6*-GFP. After the addition of CHX, the cells were lysed at 0 minutes, 30 minutes, and 90 minutes, analyzed by SDS-PAGE, and immunoblotted for α-GFP to monitor their degradation over time. WT Hrd1 cells, as predicted, saw instant suppression and degradation of Ste6*-GFP (Figure 6A, left).

Expectedly, neither of the Hrd1 mutants could support suppression in the presence of Hrd3. However, when the experiment was performed again in a *dfm1*Δ*hrd1*Δ*hrd3*Δ strain (with Hrd3 now missing), both the C399S-Hrd1 mutant and the hemi-Hrd1 mutant were able to support Ste6*-GFP degradation (Figure 6A, right). Notably, the degradation of Ste6* was not supported in the strains containing only the *hrd3*Δ null or respective mutants alone (Figure 6B). These results support the idea that Hrd1's ubiquitination function is not essential for removing an ERAD-M substrate from the ER membrane.

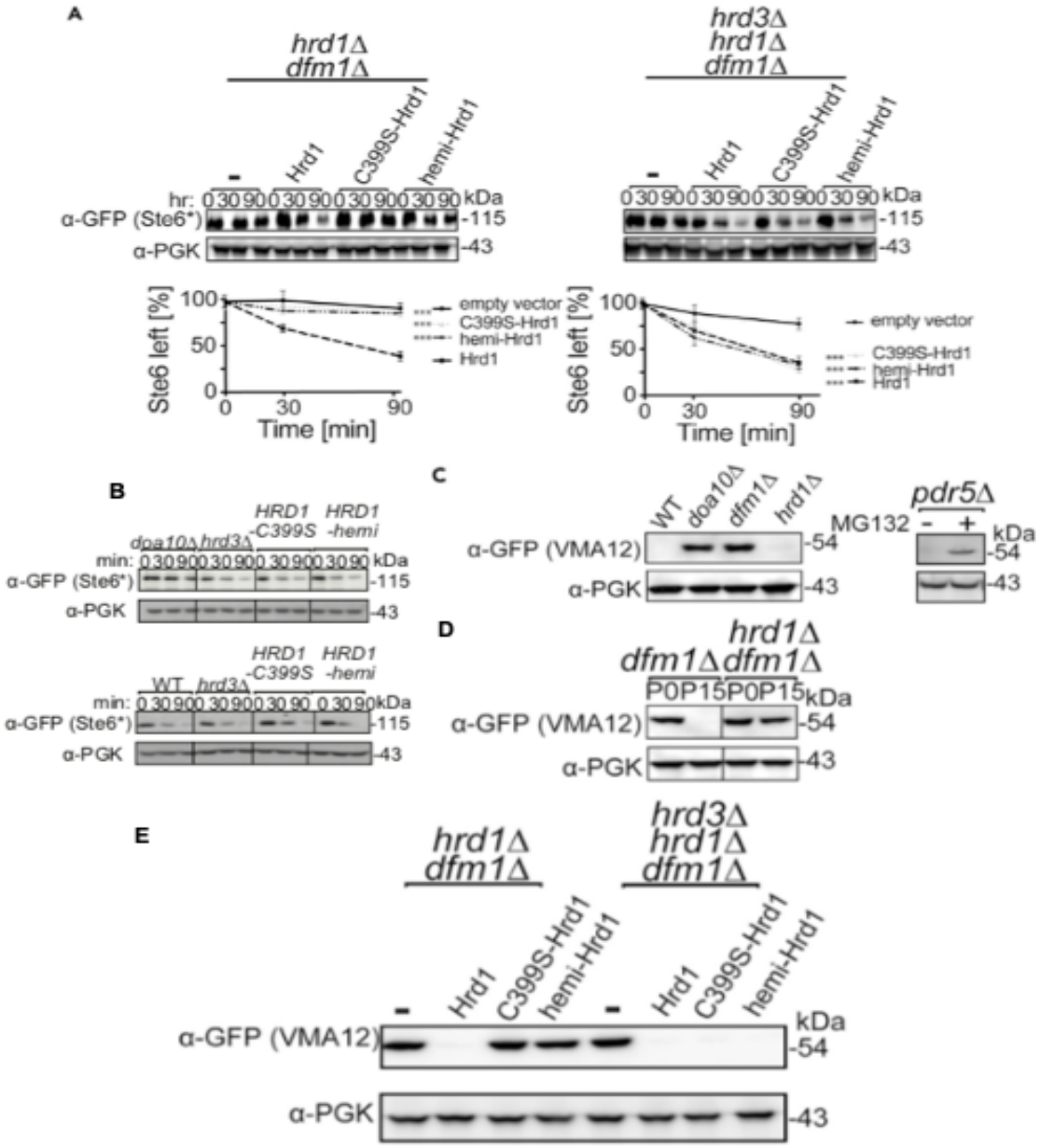

Figure 6. Hrd1's Ubiquitination Activity is Not Required for Suppressive Retrotranslocation of DOA-Dependent Substrates, Ste6* and Vma12

(A) Inactive C399S-Hrd1 and hemi-Hrd1 restores degradation of Ste6*-GFP in *dfm1*Δ*hrd1*Δ*hrd3*Δ cells. Degradation of Ste6*-GFP was measured by CHX-chase assay in test strains driven by a strong TDH3 promoter or against empty vector strains. Band intensities were normalized to PGK1 loading control and quantified by ImageJ. t=0 was taken as 100% and data are represented as mean ± SEM from at least three experiments, ***$p < 0.001$, repeated measures ANOVA. (B) *hrd3*Δ, C399S-Hrd1, and hemi-Hrd1 alone does not affect Ste6* degradation. Measured by CHX-chase assay in the indicated strains, analyzed by SDS-PAGE, and immunoblotted with α-GFP. (C) Microsomes were isolated from the indicated strains, and the steady-state levels of VMA12 were analyzed by SDS-PAGE and immunoblotted with α-GFP. (D) Steady-state levels of Vma12 were measured by western blotting in indicated strains that were either not passaged (P0) or passaged to suppression (P15). Scale bar, 5 μm. (E) C399S-Hrd1 and hemi-Hrd1 restores degradation of Vma12-GFP in *dfm1*Δ*hrd1*Δ*hrd3*Δ cells. Vma12-GFP steady-state levels analyzed by western blotting with α-GFP in indicated strains.

Hrd1's Ubiquitination Function in Removing DOA Substrate, Deg1-Vma12-GFP

Deg1-Vma12-GFP is an ER membrane protein with Deg1 fused to its N terminus, a degron recognized by the E3 ligase Doa10, thus it relies on the DOA pathway for ubiquitination and degradation. Steady state levels of Deg1-Vma12-GFP were undetectable from whole-cell lysates in our WT strains, but they were detectable in isolated microsomes. Thus, we used microsome isolations to analyze the steady-state levels of Deg1-Vma12-GFP degradation in WT cells, *doa10*Δ cells, *dfm1*Δ cells, and *hrd1*Δ cells (Figure 6C, left). *Doa10*Δ and *dfm1*Δ cells saw a presence of steady-state levels, which is expected given their role in the retrotranslocation, ubiquitination, and degradation of the substrate. However, the WT cells and *hrd1*Δ cells showed undetectable levels of Deg1-Vma12-GFP. Having Deg1 bound to it allows for rapid degradation once initiated, explaining why the GFP signal is almost invisible where the degradation occurs. These results agree with our hypothesis that this substrate does not require Hrd1 for ubiquitination or degradation. In *pdr5*Δ cells treated with proteasome-inhibitor MG132, Deg1-Vma12-GFP levels were stabilized (Figure 6C, right). This indicates the substrate is eventually degraded by the proteasome.

Microsome immunoblotting showed that by fifteen passages (P15), retrotranslocation and degradation of Deg1-Vma12-GFP were restored in the *dfm1*Δ, but not in the *dfm1*Δ*hrd1*Δ (Figure 6D). This data is consistent with the idea that the suppression is entirely dependent on Hrd1 despite its lack of role in the ubiquitination and degradation of Deg1-Vma12-GFP, since the *dfm1*Δ*hrd1*Δ double nail failed to undergo suppression even after 15 passages.

Finally, as originally proposed, studying the ERAD-M substrate Deg1-Vma12-GFP allowed us to analyze Hrd1's ubiquitination activity separate from its role in the suppressive pathway, due to its ubiquitination through the DOA pathway as well as the absence of the Hrd1-

RING domain otherwise found in SUS-GFP that potentially confounds results. Using “instant” suppression through the direct strong expression of the TDH3 promoter for our various Hrd1 test constructs, our results aligned with those of SUS-GFP. TDH3-driven native Hrd1 was able to support Deg1-Vma12-GFP degradation in the *dfm1*Δ*hrd1*Δ strain, while its mutants C399S-Hrd1 and hemi-Hrd1 could not. Contrastingly, when analyzing the *dfm1*Δ*hrd1*Δ*hrd3* versions of these three strains, Deg1-Vma12-GFP degradation was fully restored by both active and inactive versions of Hrd1 (Figure 6E). The results of the DOA pathway membrane substrates go hand in hand with those previously tested HRD pathway membrane substrates, all proving that Hrd1-mediated retrotranslocation in this alternative pathway truly does not require its catalytic ubiquitination function when Hrd3 is absent, confirming its presence is only to assist in the degradation of Hrd3.

Discussion

Neal et al. identified derlin Dfm1 as a key player in the retrotranslocation of integral membrane substrates in ERAD. Two decades ago, this key player had been published to play no role in ERAD-M; however, Neal et al. discovered that its role was so important, in fact, that a rapid suppression phenotype arises to overcome the loss of Dfm1 and continue ERAD-M in its absence (11). Through a series of experiments and analyses, they found that the E3 ligase Hrd1, of the HRD pathway and typically involved in ERAD-L, was required in this suppression. Typically, Hrd1 uses its catalytic RING domain to ubiquitinate luminal substrates. Then, alongside Dfm1's paralog Der1, it forms a channel that allows for these tagged substrates to cross over into the cytosol where they are subsequently degraded, preventing cellular stress (20). In this suppressive pathway, however, Hrd1 assists in the retrotranslocation of integral membrane substrates of ERAD, no longer playing the same role or utilizing the same parts as it requires in ERAD-L. This extends to those it works in complex with; the HRD complex is composed of Hrd1's cytoplasmic RING motif, required for ubiquitination, the mostly luminal protein Hrd3, and the protein Usa1, with its cytoplasmic Ubiquitin-like domain. Neal et al. found that neither Hrd3 nor Usa1 were required in this suppressive pathway. In fact, Hrd3 appeared to play an antagonistic role regarding the suppressed cells, serving to prevent the suppressive machinery from carrying out their function. In the absence of Hrd3, the Hrd1-mediated pathway works efficiently to perform Dfm1's otherwise lacking role, effectively restoring the retrotranslocation and degradation of ERAD-M substrates.

To understand which elements of Hrd1 are integral to this suppressive pathway, Neal et al. studied *dfm1*Δ strains expressing two mutant versions of Hrd1: the inactive C399S-Hrd1

mutant, with its essential cysteine mutated, and the hemi-Hrd1 mutant, only comprised of Hrd1's transmembrane domain without its catalytic RING domain. With Hrd3 present, neither of these mutants nor simply Hrd1 added to the *dfm1*Δ were sufficient to fully restore substrate degradation. However, with Hrd3's toxicity removed, all three strains were able to restore retrotranslocation in the suppressed strains. This data suggested Hrd1's RING domain, which serves to otherwise ubiquitinate luminal substrates in its corresponding pathway, is not necessary for this suppressive pathway; instead, the RING domain likely assists in the immediate removal of toxic Hrd3, enabling the suppressive machinery to arise.

These experiments, however, were performed using the substrate SUS-GFP, which is comprised of Hrd1's catalytic RING domain amongst others. SUS-GFP provided a powerful tool for uncoupling Hrd1's ubiquitination function from its potential retrotranslocation function, since SUS-GFP's retaining of the RING domain enables its own autoubiquitination outside of Hrd. Thus, its use allowed independent study of Hrd1's role in this suppressive pathway in the absence of its ubiquitination function. However, Gardner et al. previously demonstrated that co-expression of hemi-Hrd1 and RING-Hrd1 (which, as the name suggests, only contains Hrd1's RING domain) restored Hrd1 function in the *hrd1*Δ null through trans-expression (26). The very same issue can arise here, with SUS-GFP used as the substrate in *dfm1*Δ strains expressing hemi-Hrd1, or even C399S-Hrd1.

Our goal was to fully prove that Hrd1's ubiquitination activity is not required in the restoration of ERAD-M substrate degradation in this suppressive pathway. To address the issue posed above, we chose to analyze these strains in the context of two ERAD-M substrates ubiquitinated and degraded by the E3 ligase Doa10 of the DOA pathway. Analyzing these

substrates instead, which are entirely independent of any reliance on Hrd1, allows us to truly analyze Hrd1's ubiquitination activity without any cross interference.

The first substrate we chose to analyze was Ste6*. A well-known substrate of the DOA pathway, this multispanning substrate relies solely on Doa10 for its ubiquitination. Because it also relies on Dfm1 for its retrotranslocation across the ER membrane, Ste6* is a prime candidate for studying Hrd1's ubiquitination function independent of any confounding materials (e.g., SUS-GFP's RING domain). Expressing *dfm1*Δ*hrd1*Δ strains with either WT Hrd1, inactive C399S-Hrd1, or hemi-Hrd1 under a strong TDH3 promoter alongside our substrate Ste6*-GFP, we saw that only the WT Hrd1 was able to instantly suppress and restore the degradation of Ste6*-GFP. Neither mutant, however, was able to enact the suppressive machinery needed for this Hrd1-mediated pathway, as was expected in the presence of Hrd3. In the absence of Hrd3 through *dfm1*Δ*hrd1*Δ*hrd3*Δ strains, both mutants as well as WT Hrd1 were able to fully restore degradation of Ste6*-GFP. These results demonstrate that Hrd1's ubiquitination activity, found in its catalytic RING domain which both mutants lack, only serves to remove the obstacle that is Hrd3 in this suppressive pathway. In its absence, even those versions of Hrd1 lacking its RING domain were able to suppress the phenotype that would otherwise be displayed in the *dfm1*Δ null, once again affirming our analysis.

Two examples, however, are better than one, which is why we tested a second substrate, Deg1-Vma12-GFP. Another well-characterized DOA-dependent substrate, Deg1-Vma12-GFP is an ER membrane protein with Deg1 fused to its N-terminus. Deg1 is a degron recognized by the E3 ligase Doa10, thus rendering it a substrate that is ubiquitinated and degraded by the DOA pathway. Because steady-state levels of Deg1-Vma12-GFP were undetectable from whole-cell yeast lysates in our wild-type strains, we chose to perform microsome isolation preparations,

where they were noticeably detectable. Steady-state levels of the Doa10 substrate were detectable in both the *doa10*Δ and *dfm1*Δ cells, which is expected given their roles in its ubiquitination, retrotranslocation, and degradation. Deg1-Vma12-GFP levels were also stabilized in *pdr5*Δ cells treated with proteasome-inhibitor MG132, indicating the substrate is eventually degraded by the proteasome. Co-expressing *dfm1*Δ*hrd1*Δ cells and only *dfm1*Δ cells with Deg1-Vma12-GFP saw restoration of retrotranslocation and degradation by fifteen passages only in the *dfm1*Δ, once again showing Hrd1's role in the suppressive pathway that arises in Dfm1's absence. Furthermore, using "instant" suppression as before through the direct strong expression of the TDH3 promoter for our WT Hrd1, C399S-Hrd1, and hemi-Hrd1 constructs, our results aligned with those of both SUS-GFP and Ste6*-GFP. In the *dfm1*Δ*hrd1*Δ*,* only WT Hrd1 was able to fully restore degradation of Deg1-Vma12-GFP where our two mutants could not, likely due to Hrd3's presence. In the absence of Hrd3, all three constructs were able to accordingly restore retrotranslocation and degradation of the substrate. These results once again prove that Hrd1's catalytic RING domain, usually for ubiquitinating ERAD-L substrates, only exists in this suppressive pathway to immediately remove the toxic Hrd3.

Through the use of *dfm1*Δ*, dfm1*Δ*hrd1*Δ*,* and *dfm1*Δ*hrd1*Δ*hrd3*Δ strains expressing WT Hrd1, C399S-Hrd1, and hemi-Hrd1, we were able to prove that Hrd1's ubiquitination activity is dispensable in this Hrd1-mediated suppressive pathway. We first demonstrated this using SUS-GFP, an autoubiquitinating substrate that allowed for study of Hrd1 independent of its ubiquitination function, and then subsequently using Doa10 substrates Ste6* and Vma12, to provide evidence where SUS-GFP could otherwise confound. The implications of this data are extensive, adding a new dimension of understanding to the E3 ligase Hrd1 and the functional plasticity of the well-studied HRD complex. Dfm1 plays a key mediator in the retrotranslocation

of ERAD-M substrates from both the HRD and DOA pathways. However, in its absence, retrotranslocation is fully restored by a rapid suppression mechanism that masks the expected phenotype, implying a separate and efficient route for retrotranslocation to still occur. In this alternate pathway, elevation of Hrd1 appeared as a central feature of suppression, indicating its ability to participate in ERAD-M in some conditions despite its usual non-participation in this branch. The above studies of *dfm1*Δ suppressees reveals the HRD complex undergoes remodeling allowing the restoration and continuation of ERAD-M. Hrd1, a large protein responsible for ubiquitinating luminal substrates in ERAD-L, adapts itself in the absence of Dfm1. The elevation of Hrd1 appears to cause remarkable remodeling of the HRD complex, allowing for immediate removal of obstacle Hrd3 and enabling it to expand its function to include the lacking dfm1's retrotranslocation function. These results demonstrate the remarkable functional plasticity of this well-conserved pathway, eliciting further questions: How does elevation of Hrd1 lead to conversion of Hrd3 from an otherwise stable ERAD-L comrade to a toxic, rapidly degraded substrate? How does the Hrd1 gene adapt to take on this new function it did not previously appear to have? What features of Hrd1 are important for replacing Dfm1, and do any structural features of rhomboids also exist in the Hrd1 transmembrane domain allowing for this suppression? Despite these many questions, it is evident that from these studies that ERAD machinery is highly capable of adaptation and functional flexibility to accommodate other known and potentially unknown cellular stresses.

Chapter 1, in full, is a reprint of the material as it appears in iScience 2020. Neal, Sonya E, Nejatfard, Anahita, CellPress 2020. The thesis author was the third author on this paper.

Chapter 2: Yeast Derlin Dfm1 Structure and Function

Derlin Dfm1 Belongs to the Rhomboid Superfamily

As mentioned in Chapter 1, Neal et al. explored membrane substrate retrotranslocation by screening a complete collection of yeast mutants via SPOCK (single-plate orf compendium kit), which consisted of a 5,808-yeast strain array of non-essential gene deletion mutants and essential DAmP gene mutants, for deficiencies in degradation of SUS (self-ubiquitinating substrate)-GFP. Through this study, they were able to determine yeast derlin Dfm1 plays a role as a mediator of retrotranslocation for multi-spanning membrane substrates in ERAD (11). As mentioned, this contradicted previous findings that Dfm1 had little to no role in ERAD; this was resolved by finding that the loss of Dfm1 alongside strong expression of membrane substrates imposed a growth stress on cells, which triggered the rapid and complete rise of suppressive machinery masking the loss of its function (11).

Sequence and structural homology studies have shown that derlins, including Dfm1, belong to the rhomboid superfamily (18). As discussed, the rhomboid family is known for its involvement in many membrane-related processes, including development, signaling, protein trafficking, and protein quality control (2). They are typically intermembrane proteases that cleave membrane substrates within the lipid bilayer via their serine-histidine dyad active site (2, 22, 27). A large subclass of the rhomboid family, of which derlins belong to, are known as rhomboid pseudoproteases, due to their lack of proteolytic residues (17). Despite this lack of proteolytic activity, rhomboid pseudoproteases have retained conserved rhomboid residues, likely enabling them to utilize specific rhomboid features for executing their various functions. For instance, human and yeast derlins have the widely conserved WR and GxxxG rhomboid

motifs, allowing them to remove substrates across the membrane (18, 11). Accordingly, research into the structure and associated functions of these conserved residues is highly important as it can reveal insight into the roles and mechanisms of rhomboids across all domains of life.

Analogous Studies on Rhomboid Structure

Structural studies of rhomboid protease GlpG found in bacteria *E. coli* and *H. influenzae* along with other mechanistic studies on the rhomboid superfamily have yielded insight into some mechanistic features that may play a role in derlin-mediated retrotranslocation (27, 28). Bacterial rhomboids possess a compact architectural fold that is presumed to induce local perturbations of the lipid bilayer to facilitate interactions with substrates prior to cleavage (22). Through Cryo-EM work, Dfm1's yeast paralog, Der1, has been found to induce lipid thinning, which assists in its role retrotranslocating luminal ERAD substrates in the ERAD-L pathway (20). Specifically, the authors demonstrated that Der1 forms a half channel alongside E3 ligase Hrd1 to induce lipid thinning, facilitating in the retrotranslocation of ERAD-L substrates. An intriguing possibility is that Dfm1 has retained this membrane perturbing property, enabling it's the extraction of ERAD-M substrates from the ER membrane.

Beyond the potential lipid perturbing property, the structural features of rhomboids along with their conserved residues can yield a significant amount of mechanistic insight. The core of GlpG, like other rhomboid proteins, is composed of a six transmembrane (TM) compact helical bundle and employs a catalytic dyad to hydrolyze peptide bonds, with a serine acting as a nucleophile and a histidine acting as the general base (27). An interesting structural feature of a rhomboid protein is a long loop region between their first and second transmembrane domains, known as Loop 1 (L1) (27). This loop is partially submerged in the top region of the membrane

due to hydrophobic residues that line the lower portion of the loop. It is thought that this hairpin loop optimally positions the rhomboid in the correct orientation in the membrane to perform its catalytic duties (27, 28). The L1 region also shows the highest sequence conservation across proteases; it is here that the crucial WR motif can be found (17, 28).

Derlin Dfm1 also contains the highly conserved WR motif in L1 as well as the conserved GxxxG motif in TM6, both of which have been shown to be important for rhomboid derlin retrotranslocation function (11, 18) (Figure 7A). This begged the question of whether these motifs are sufficient for Dfm1 retrotranslocation. Neal et al. examined this using a Der1-SHP chimera, which consists of Dfm1's closest homolog Der1 fused to Dfm1's cytoplasmic SHP tail (Figure 7B). Previously, they revealed that the Der1-SHP chimera can support Cdc48 recruitment by binding Cdc48 through its SHP tail; however, Der1's transmembrane segment is unable to support retrotranslocation (Figure 7B). Der1's transmembrane region does not possess those highly conserved WR and GxxxG motifs; instead, it harbors GR and NxxxG instead (Figure 7C). To study whether those motifs are sufficient for Der1-SHP to retrotranslocate substrates, both motifs were inserted at homologous sites within the Der1-SHP transmembrane region, generating the Der1-SHP-WR mutant, the Der1-SHP-GxxxG mutant, and the Der1-SHP-WR+GxxxG mutant. All three mutants were able to support Cdc48 recruitment similar to the unaltered Der1-SHP-chimera protein through a Cdc48 microsome association assay (Figure 7D, 7F). However, none of the mutants was able to facilitate the degradation of bona fide ERAD-M substrate Hmg2-GFP (Figure 7E). This points to other residues in Dfm1's transmembrane region to be required for retrotranslocation.

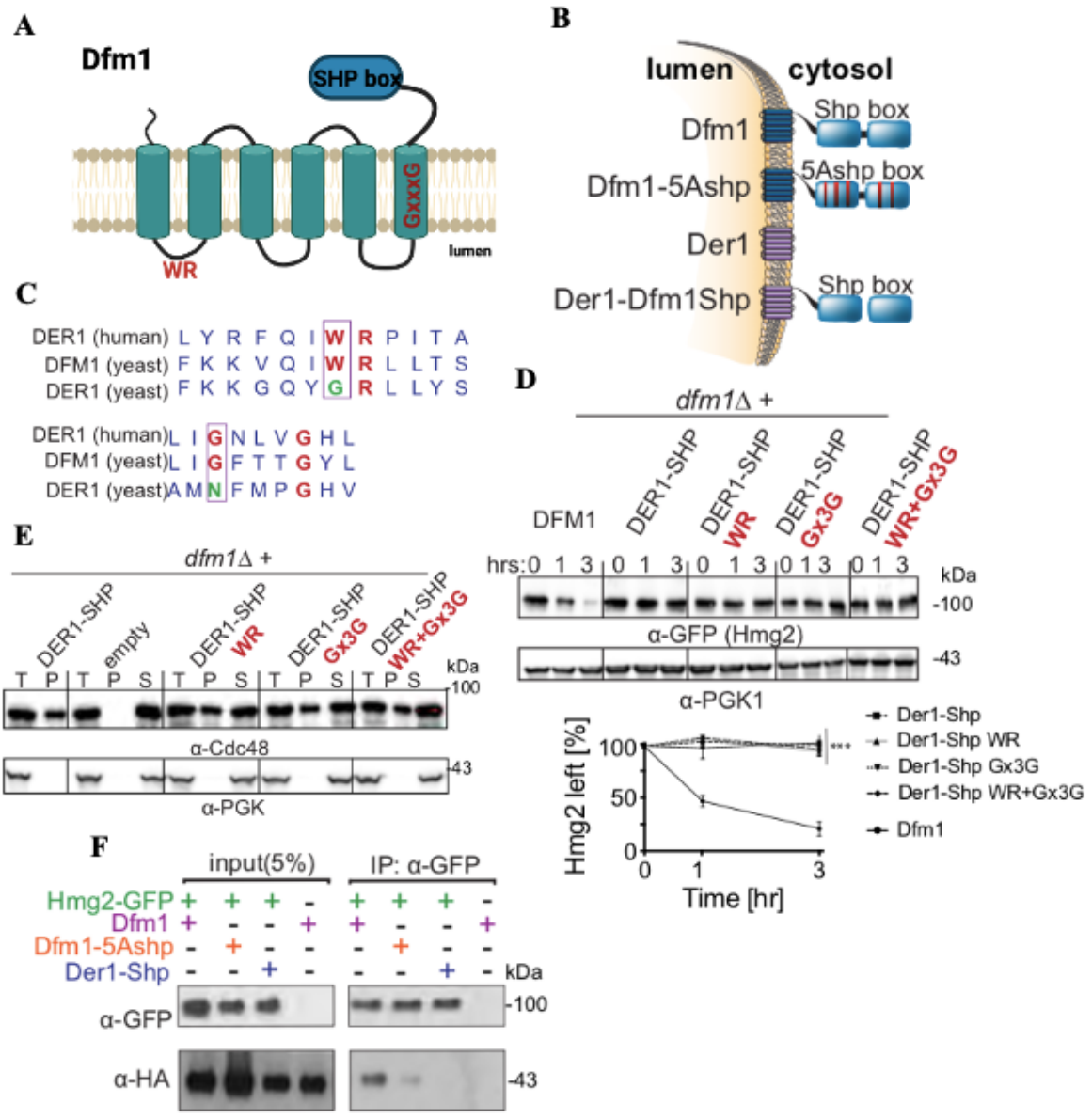

Figure 7. WR and GxxxG are Not Sufficient for ERAD-M Retrotranslocation.
(A) Depiction of Dfm1. Dfm1 has WR motif in the first luminal loop and a GxxxG dimerization motif in TMD6. (B) Depiction of Dfm1, Der1, and Der1-SHP. Dfm1 and Der1 are ER-localized membrane proteins with six transmembrane domains. Unlike Der1, Dfm1 has an extended cytoplasmic tail containing two SHP boxes. (C) Alignment of WR and GxxxG motif from *H. sapiens* Derlin-1 and *S. cerevisiae* Der1 and Dfm1. (D) The WR and GxxxG motifs within Der1-SHP are not sufficient for Hmg2 degradation. In the indicated strains, degradation of Hmg2-GFP was measured by CHX-chase assay. Cells were analyzed by SDS-PAGE and immunoblotted for Hmg2-GFP with α-GFP. Band intensities were normalized to PGK1 loading control and quantified by ImageJ. t=0 was taken as 100% and data is represented as mean ± SEM from at least three experiments, ***$p < 0.001$, Repeated Measures ANOVA. (E) The WR and GxxxG motifs within Der1-SHP does not disrupt Cdc48 recruitment. Total cell lysate (T) from the indicated strains was separated into soluble cytosolic fraction (S) and pellet microsomal fraction (P) upon centrifugation at 14,000 x g. Each fraction was analyzed by SDS-PAGE and immunoblotted with α-Cdc48 and α-PGK1 for control. (F) Hmg2 binding to Dfm1-5Ashp and Der1-SHP analyzed by co-IP. The IP was analyzed for the presence of Hmg2.

Salient questions arise: What structural features of Dfm1 lend to its function, and do these features interfere with Dfm1's ability to retrotranslocate membrane substrates in ERAD? Does Dfm1 employ the same lipid distortion function for retrotranslocation?

Study Aims and Goals

To address these questions, we performed a non-biased sequence analysis of Dfm1 coupled with cellular assays and computational analyses to characterize the mechanistic features that are critical for Dfm1's actions. Thus, our first goal was to identify a subset of retrotranslocation-deficient Dfm1 mutants. These findings provide a mechanistic insight into other members of the rhomboid superfamily, providing a conceptual framework for others studying what role these conserved residues of their potential rhomboids of interest can be studied. Our second goal is to determine whether Dfm1 also retains the lipid thinning functions of its bacterial counterpart and yeast paralog through molecular dynamic simulations.

My hypothesis is that Dfm1 has retained conserved rhomboid residues that aid in both its membrane perturbing properties as well as its removal of multi-spanning membrane substrates in ERAD-M.

Materials and Methods

Yeast and Bacteria Growth Media

Standard yeast Saccharomyces cerevisiae growth media were used as previously described in Chapter 1, including YPD medium and SC media supplemented with 2% dextrose and amino acids to enable growth of auxotrophic strains at 30°C. *Escherichia coli* Top10 cells were grown in standard LB media with ampicillin at 37°C.

Plasmids and Strains

Plasmids used in this study are listed in Table 3. Plasmids for this work were generated using standard molecular biology techniques and verified by sequencing (Eton Bioscience, Inc.). A complete list of yeast strains and their corresponding genotypes are listed in Table 4. All strains used in this work were derived from S288C or Resgen. Yeast strains were transformed with DNA or PCR fragments using the standard LiOAc method. Null alleles were generated by using PCR to amplify a selection marker flanked by 50 base pairs of the 5' and 3' regions, which are immediately adjacent to the coding region of the gene to be deleted. The selectable markers use for making null alleles were genes encoding resistance to G418 or CloNAT/nourseothricin. After transformation, strains with drug markers were plated onto YPD followed by replica-plating onto YPD plates containing 500 μg/mL G418 or 200 μg/mL nourseothricin. All gene deletions were confirmed by PCR.

Table 3. List of Plasmids Used in this Thesis, Related to Figures 8-11

Plasmid	Plasmid Type	Yeast Marker	Gene
pSN59	YCp	LEU2	pDFM1-F107S
pSN60	YCp	LEU2	pDFM1-L64V
pSN90	YCp	LEU2	pDFM1
pSN93	YCp	LEU2	pDFM1-K67E
pSN94	YCp	LEU2	pDFM1-Q101R
pSN95	YCp	LEU2	pDFM1-F58S
pSN115	YIp	TRP1	pSUS-GFP
pRH613	YIp	URA3/ADE2	pTDH3-HMG2-GFP
pRH2058	2 μ	URA3	pPGK-STE6-166-3HA-GFP

Table 4. List of Yeast Strains Used in this Study, Related to Figure 8-11

Strain	Genotype
SEN 112	Mata *ade2-101 met2 lys2-801 his3Δ200 trp1::hisG leu2Δ ura3-52::URA3::TDH3pr-SUS-GFP dfm1Δ::KanMX hrd1Δ::NatR*
SEN 182	Mata *ade2-101 met2 lys2-801 his3Δ200 trp1::hisG leu2Δ ura3- 52 dfm1Δ::KanMX CEN::HIS3:PDR5*-HA*
SEN 198	Mata *ade2-101 met2 lys2-801 his3Δ200 trp1::hisG leu2Δ ura3- 52 dfm1Δ::KanMX CEN::URA3::STE6-166-HA-GFP*

dfm1Δ strain handling

To observe the phenotypic effect of *dfm1Δ* null strains, freshly transformed *dfm1Δ* null cells with the respective ERAD-M substrates was used in every assay.

Homology Modeling

To build the 3D model of yeast derlin, Dfm1 protein on the template of yeast derlin Der1, the Phyre2 system was utilized (29). Initially, the primary sequence is scanned against a database of 10 million known sequences for homologs via PSI-Blast. From here, homologous sequences are organized into an evolutionary fingerprint through Hidden Markov Models. Evolutionary fingerprints and Hidden Markov Models are made for the 65,000 known 3D structures to create a database of known structures. A scan of the evolutionary fingerprint with the database creates an alignment to known structures ranked by confidence of homology. This alignment generates a

3D threaded model with excellent accuracy even when sequence identity is less than 15%, and in addition is able to reliably detect extremely remote homology (29).

Random Mutagenesis of Dfm1

pRH2013 plasmid containing DFM1 driven from its native promoter was amplified by PCR using a high fidelity Phusion polymerase (control) and error prone Mutazyme 2 to introduce point mutations into DFM1. Specifically, 500ng of template DNA (pRH2013) and 20 cycles of PCR were used to obtain an average of 1-3 point mutations within DFM1, excluding the genetic region encoding the SHP motifs as per protocol instructions. Mutagenized DFM1 was amplified using high fidelity Phusion polymerase and treated with Dpn1 at 37^{o}C overnight to digest the original unmutagenized template followed by PCR cleanup of mutagenized DFM1 using Promega wizard PCR cleanup kit. In parallel, backbone plasmid from pRH2013 was prepared by overnight digestion with Spe1 and PshA1 and then purified from 0.8% agarose gel. For homologous recombination of mutagenized DFM1 with pRH2013 backbone, linearized pRH2013 and purified mutagenized DFM1 were co-transformed into *dfm1*Δ*hrd1*Δ yeast cells containing TDH3pr-SUS-GFP using a 1:9 backbone to insert ratio. Recombinants were selected on SC-Leu and incubated at 30^{o}C. Resulting transformants were selected for high colony fluorescence, indicating their inability to degrade the optical retrotranslocation reporter, SUS-GFP. Plasmids were recovered from selected yeast transformants and transformed into E. coli. Plasmids were recovered using Promega Wizard Plus SV Miniprep kit, as per manufacturer's protocol and sent to ETON for sequencing using T7 (forward) and T3 (reverse) universal primers. Results for sequencing were aligned to wildtype DFM1 and mutated regions were

identified using in house python scripts. Mutants containing one point mutation and no early stop codons verified by both forward and reverse strands were selected as mutants of interest.

Plasmid Recovery from Transformants

Plasmid extractions was performed as described in (30). Transformants were inoculated into 3-ml YPD and grown overnight. The following day, 1 ml of YPD was added to stationary phase cultures, which were then allowed to grow for an hour at 30°. The entire culture was then pelleted and resuspended in 250 µl of resuspension buffer from a Promega Wizard Plus SV Miniprep kit (A1460). Resuspended cells were lysed with beads for 5 min in a multi- vortexer. Lysed cells and supernatant were then collected by nesting the microcentrifuge tube into a 15-ml conical tube, piercing the 2-ml microcentrifuge tube with a needle, and spinning the nested tubes at 2,000 rpm for 2 min. Lysed cells and cell lysate were then thoroughly resuspended, and the remainder of the miniprep was carried out according to the manufacturer's protocol.

in vivo Retrotranslocation Assay

in vivo retrotranslocation assay was performed as described in (Neal et al., 2019). Cells in log phase (OD_{600} 0.2-0.3) were treated with MG132 (benzyloxycarbonyl-Leu-Leu-aldehyde, Sigma) at a final concentration of 25 µg/mL (25 mg/mL stock dissolved in DMSO) for 2 hours at 30ºC and GGPP (Geranylgeranyl pyrophosphate ammonium salt, Sigma) at a final concentration of 11 µM for 1 hour at 30ºC and 15 ODs of cells were pelleted. Cells were resuspended in H_20, centrifuged, and lysed with the addition of 0.5 mM glass beads and 400 µL of XL buffer (1.2 M sorbitol, 5 mM EDTA, 0.1 M KH_2PO_4, final pH 7.5) with PIs, followed by vortexing in 1minute intervals for 6-8 min at 4ºC. Lysates were combined and clarified by centrifugation at 2,500 x g

for 5 min. Clarified lysate was ultracentrifuged at 100,000 x g for 15 min to separate pellet (P100) and supernatant fraction (S100). P100 pellet was resuspended in 200 µL SUME (1% SDS, 8 M Urea, 10 mM MOPS, pH 6.8, 10 mM EDTA) with PIs and 5 mM N-ethyl maleimide (NEM, Sigma) followed by addition of 600 µL immunoprecipitation buffer (IPB) with PIs and NEM. 100 supernatant was added directly to IPB with PIs and NEM. 15 µL of rabbit polyclonal anti- GFP antisera (C. Zuker, University of California, San Diego) was added to P100 and S100 fractions for immunoprecipitation (IP) of Hmg2-GFP. Samples were incubated on ice for 5 minutes, clarified at 14,000 g for 5 min and removed to a new eppendorf tube and incubated overnight at 4ºC. 100 µL of equilibrated Protein A-Sepharose in IPB (50% w/v) (Amersham Biosciences) was added and incubated for 2 hours at 4ºC. Proteins A beads were washed twice with IPB and washed once more with IP wash buffer (50 mM NaCl, 10 mM Tris), aspirated to dryness, resuspended in 2x Urea sample buffer (8 M urea, 4% SDS, 1mM DTT, 125 mM Tris, pH 6.8), and incubated at 55ºC for 10 min. IPs were resolved by 8% SDS-PAGE, transferred to nitrocellulose, and immunoblotted with monoclonal anti-ubiquitin (Fred Hutchinson Cancer Center, Seattle) and anti-GFP (Clontech, Mountain View, CA). Goat anti-mouse (Jackson ImmunoResearch, West Grove, PA) and goat anti-rabbit (Bio-Rad) conjugated with horseradish peroxidase (HRP) recognized the primary antibodies. Western Lightning® Plus (Perkin Elmer, Watham, MA) chemiluminescence reagents were used for immunodetection.

Cycloheximide-Chase Assay

For yeast cells, cycloheximide chase assays were performed as previously described (Sato et al., 2009). Cells were grown to log-phase (OD_{600} 0.2-.03) and cycloheximide was added to a final concentration of 50 µg/mL. At each time point, a constant volume of culture was

removed and lysed. Lysis was initiated with addition of 100 µl SUME with PIs and glass beads, followed by vortexing for 4 min. 100 µl of 2xUSB was added followed by incubation at 55°C for 10 min. Samples were clarified by centrifugation and analyzed by SDS-PAGE and immunoblotting.

Native co-Immunoprecipitation

Cultures from various yeast strains were grown to OD_{600} .2-.45 and 15 ODs of cells were pelleted, rinsed with H_20, and lysed with 0.5 mM glass beads in 400 µL of MF buffer supplemented with protease inhibitors. This was followed by vortexing at 1-minute intervals for 6-8 minutes at 4°C. Lysates were combined and clarified by centrifugation at 2,500 x g for 5 min followed by centrifugation at 14,000 x g for 15 min to obtain the microsomal pellet. The microsomal pellet was resuspended in 1 mL of Tween IP buffer (500 mM NaCl, 50 mM Tris, pH 7.5, 10 mM EDTA. 1.5% Tween-20) and incubated on ice for 30 minutes. Lysates were then centrifuged for 30 min at 14,000 x g, and the supernatant was incubated overnight with 10 µL of equilibrated GFP-Trap® agarose (ChromoTek Inc., Hauppauge, NY) at 4°C. The next day, the GFP-Trap® agarose beads were combined to one tube, washed once with non-detergent IP buffer, washed once more with IP wash buffer, and resuspended in 100 µL of 2xUSB. Samples were resolved on 8% SDS-PAGE and immunoblotted for ubiquitin with anti-Ub, Cdc48 with α-CDC48, Hmg2-GFP with α-GFP, Dfm1-HA with α-HA, and Ste6*-GFP with α-GFP.

Results

Yeast Dfm1 Retains Highly Conserved Rhomboid and Derlin-Specific Residues

Sequence alignment of Dfm1 and other rhomboid family members uncovers Dfm1 contains residues beyond the conservation of Trp136 and Arg137, the residues that compose the WR motif. In fact, there are a series of well-conserved residues found across the rhomboid family, from the bacterial GlpG but also mammalian rhomboids Derlin-1, Derlin-2, Derlin-3, and RHBDL4 (Figure 8A; *highlighted in red and orange*). Beyond those common rhomboid features, the sequence alignment also reveals Dfm1 has residues that are conserved and retained specifically in mammalian derlin rhomboid pseudoproteases (Figure 8A; *circled in orange*). We chose to study these residues to understand how Dfm1 utilizes its rhomboid and derlin-specific features for its retrotranslocation role in ERAD of membrane substrates.

Dfm1's L1 and TM2 Mutants Incapable of Supporting its Retrotranslocation Function

To identify additional residues that may play a role in Dfm1's retrotranslocation function, a previous graduate student performed a sequence analysis screen where Dfm1's transmembrane segment was randomly mutagenized. Only the transmembrane region was altered, and not the cytoplasmic SHP tail, to prevent false positives that may arise from disruption of Dfm1's Cdc48 recruitment function. Random mutagenesis was performed using the GeneMorph II random mutagenesis kit. Those mutants were then introduced into *dfm1*Δ*hrd1*Δ double null yeast cells that also contained the self-ubiquitinating substrate, SUS-GFP (Figure 9A, 9B). As referenced in Chapter 1, it was essential for hrd1 to also be absent in this strain since it is able to restore retrotranslocation when Dfm1 is absent (9, 11). Transformants were then screened for high

colony fluorescence, indicating buildup of SUS-GFP due to an inability to retrotranslocate it. Plasmids were generated from those highly fluorescent strains and sequenced to determine the underlying Dfm1 mutation. Dfm1 mutants with no premature stop codons and a single mutation were those to be analyzed further for their stability; if robustly expressed, those mutants were subjected to cellular fractionation and Cdc48 binding assays to indicate those mutants that correctly localized to the ER and did not disrupt in Cdc48's recruitment activity (Figure 8B-D). Because Dfm1 also associates with the HRD complex in ERAD-M, which includes the E3 ligase Hrd1 and its partner protein Hrd3, the graduate student validated that the five mutants that passed all these screens did not disrupt their association with the major components of the HRD complex (Figure 8E).

We next generated a structural model of Dfm1 and these uncovered mutants using homology modeling of Der1, Dfm1's isoform that Wu et al. were able to solve the structure of (20). The homology model revealed the Dfm1 mutants to be enriched in both L1 (with mutants F58S, L64V, and K67E) as well as TM2 (with Q101R and F107S, respectively) (Figure 9C, 9D, and Figure 8A; *blue asterisks*). As the sequence alignment shows, the leucine at position 64 and lysine at position 67 of Dfm1 are conserved across the rhomboid family, while the phenylalanine at position 107 is conserved specifically among derlins (Figure 8A).

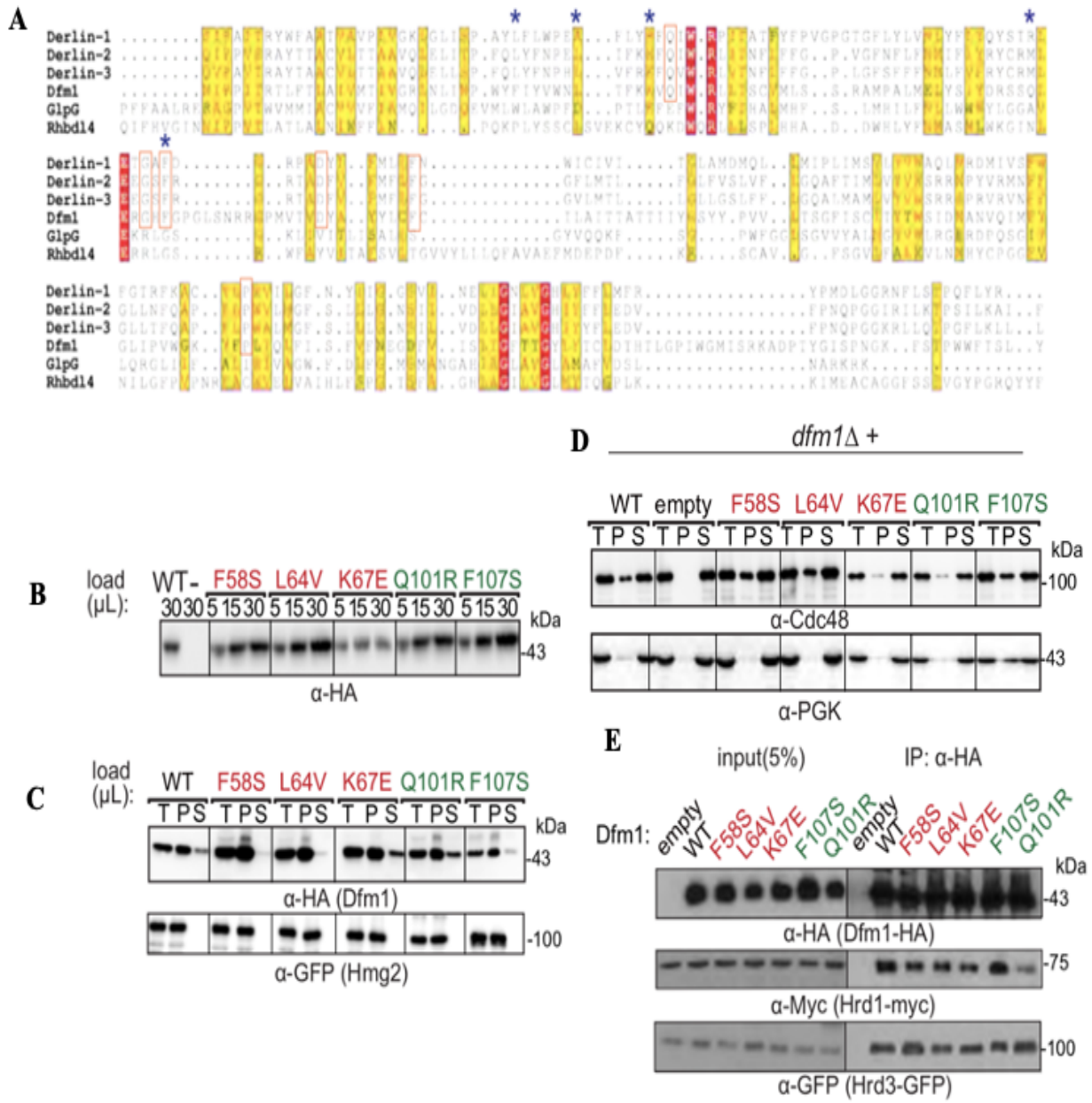

Figure 8. Sequence Analysis and Validation of Retrotranslocation-Deficient Mutants
(A) Dfm1 is a rhomboid pseudoprotease. TCoffee alignment of the transmembrane regions of Derlin-1, Derlin-2, Derlin-3, and RHBDL4 from *H. sapiens*; Dfm1 from *S. cerevisiae*; and GlpG from *E. coli*. Identically and similarly conserved residues are highlighted in red and yellow respectively. Residues selected from loss of function screen are indicated by blue asterisks. (B) Stability of Dfm1 mutants was measured by loading increasing amounts of lysates (5 μL, 15 μL, and 30 μL) on SDS-PAGE followed by immunoblotting with α-HA. (C) Dfm1 mutants localize to the ER. Total cell lysate (T) from indicated strains were separated into soluble cytosolic fraction (S) and pellet microsomal fraction (P) upon centrifugation at 14,000 x g. Each fraction was analyzed by SDS-PAGE and immunoblotted for Dfm1 mutants with α-HA and ER-localized Hmg2 with α-GFP. (D) Dfm1 mutants do not disrupt its Cdc48 recruitment function. Same as (C) except Cdc48 recruitment was analyzed by immunoblotting with α-Cdc48 and α-PGK1 for control. (E) Association of retrotranslocation-deficient mutants to E3 ligase Hrd1 and Hrd3 was analyzed by co-IP. As a negative control, cells not expressing Dfm1 were used.

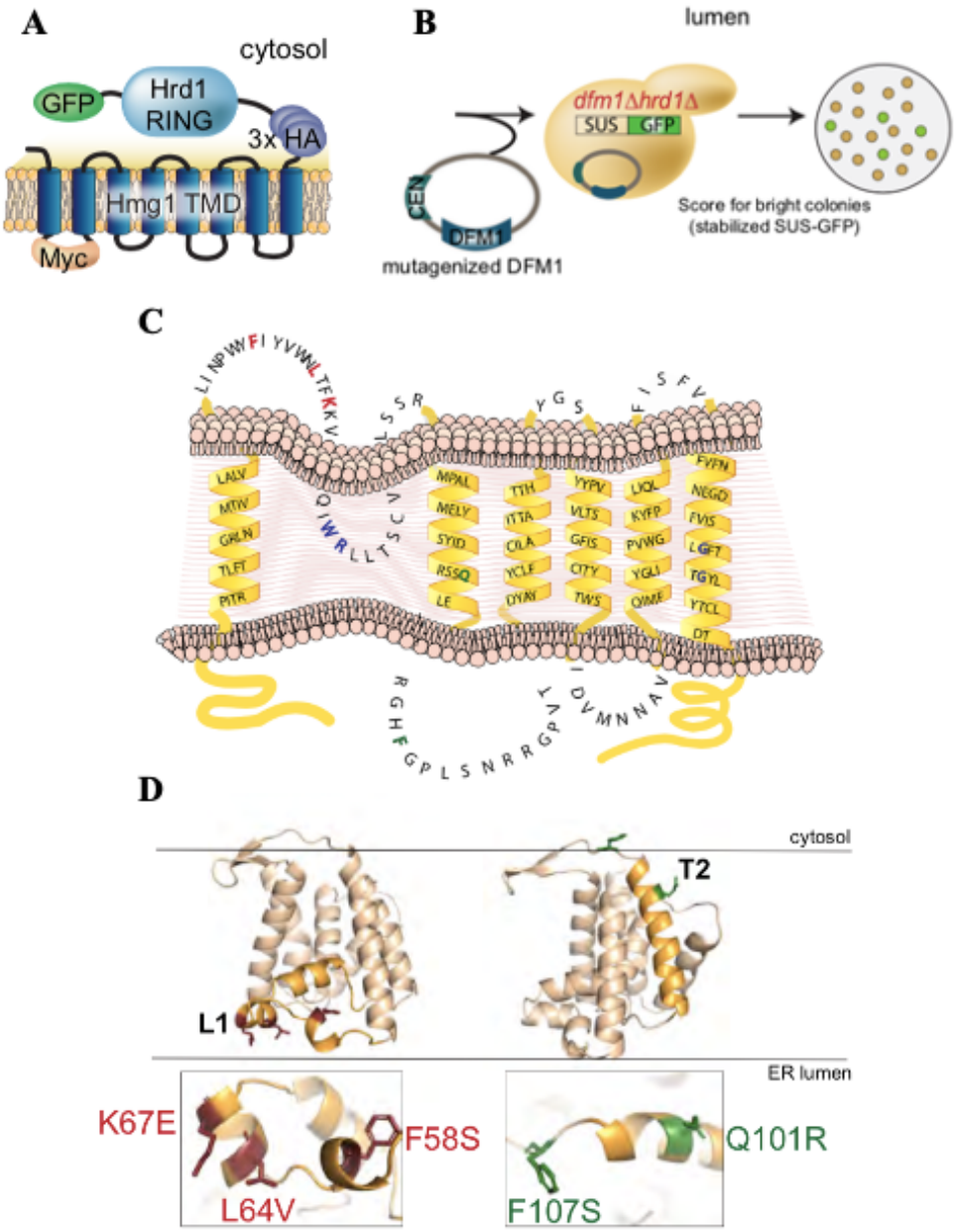

Figure 9. Dfm1 is Intolerable to Mutations in Loop 1 and Transmembrane Domain 2
(A) Depiction of fusion protein, SUS-GFP. The transmembrane Hmg1 domain has a lumenal Myc epitope and the cytosolic domain has three HA epitopes followed by the HRD RING domain fused with the GFP epitope. (B) Full-length Dfm1 (except for region encoding SHP box) was subjected to random mutagenesis. Mutagenized Dfm1 was transformed into *dfm1*Δ*hrd1*Δ cells expressing SUS-GFP and scored for stabilization of SUS-GFP or high colony fluorescence by visualization. (C) Depiction of Dfm1 mutants (indicated in red for L1 and green for TM2) that were selected from the random mutagenesis screen and validated for expression and ability to localize to ER and recruit Cdc48. (D) Homology model of Dfm1. Positions of L1 and TM2 mutants are indicated in red and green respectively.

Dfm1's L1 and T2 Mutants Affect Retrotranslocation of ERAD-M Substrates

Once the graduate student validated the set of Dfm1 mutants, it set the stage for us to examine the possible role of these Dfm1 mutants and how they affect the ERAD of various membrane substrates. First, the mutants were directly tested with CHX-chase assays separately on integral membrane HRD pathway substrates Hmg2 and Pdr5* as well as integral membrane DOA pathway substrate Ste6* (Figure 10A-C). Hmg2 and Ste6*, which would be otherwise degraded under normal ERAD-M conditions, were stabilized by each Dfm1 mutant. The substrate Pdr5*, however, was observed to undergo partial degradation in the presence of each mutant. This was likely due to the rapid suppressive nature of Dfm1 mutants seen to be triggered by the overexpression of ERAD-M substrates, as mentioned in Chapter 1 (9, 11). Regardless, Pdr5* saw a slower degradation rate by the Dfm1 mutants when compared to WT Dfm1. These results demonstrate that the Dfm1 mutants we derived from the genetic screen affected the degradation of ER membrane substrates.

To investigate whether Hmg2 and Ste6* retrotranslocation was affected by the Dfm1 mutants, we analyzed the substrates in the presence of the mutants using the *in vivo* retrotranslocation assay (Figure 10D, 10E). WT Dfm1 with its normal function intact saw buildup of ubiquitinated Hmg2 and Ste6* in the supernatant (S) fraction. Buildup in the supernatant was expected due to the imposed inhibition of proteasome function by MG132 on the cells, allowing study of retrotranslocation without any substrate degradation. Contrastingly, when the same experiment was performed on each of the Dfm1 mutants, buildup of ubiquitinated Hmg2 and Ste6* was seen in the microsomal pellet (P) fraction, indicating retrotranslocation into the cytosol did not occur. The inhibition of retrotranslocation was comparable to control strains where Dfm1 was

absent. These results reveal that not only are the Dfm1 L1 and TM2 mutants dysfunctional in ERAD, but they are also dysfunctional in retrotranslocation.

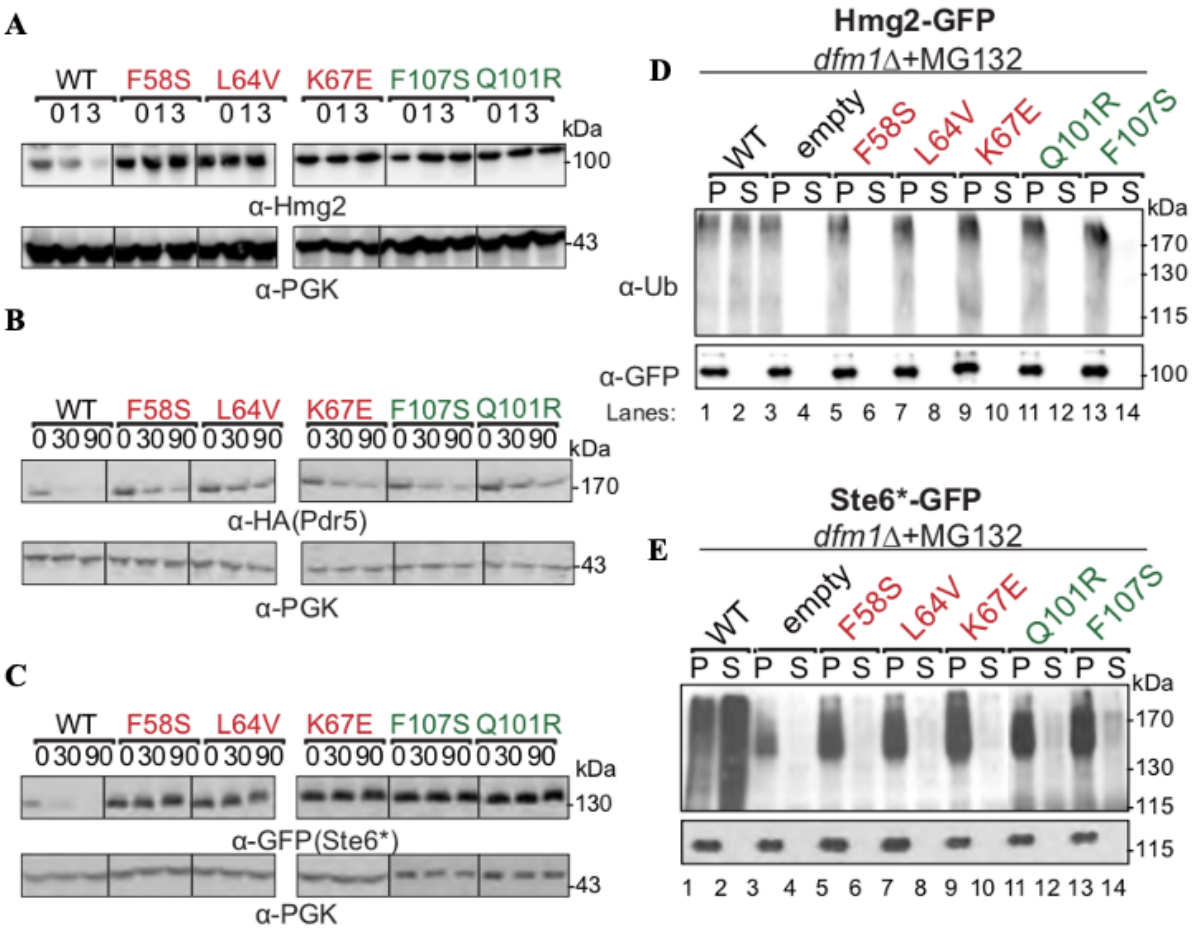

Figure 10. Dfm1 Mutants are Defective in ERAD-M Retrotranslocation and Degradation
(A) *dfm1*Δ strains expressing the indicated Dfm1 mutants were grown to log-phase and degradation was measured by CHX. After CHX addition, cells were lysed at the indicated times and analyzed by SDS-PAGE and immunoblotted for Hmg2-GFP with α-GFP. (B) Same as (A) expect degradation of Pdr5*-HA was measured in indicated strains. (C) Same as (A) except degradation of Ste6*-GFP was measured in indicated strains. (D) Dfm1 mutants are required for retrotranslocation of Hmg2-GFP. Indicated strains were grown to log-phase and treated with MG132 prior to lysis. Crude lysate was prepared from each strain and ultracentrifuged to discern ubiquitinated Hmg2-GFP that either has been retrotranslocated into the soluble fraction (S) or remained in the membrane (P). Following fractionation, Hmg2-GFP was immunoprecipitated from both fractions, resolved on 8% SDS-PAGE and immunoblotted with α-GFP and α-Ubi. (E) Same as (D) except in vivo retrotranslocation assay was performed on Ste6*-GFP.

Dynamic Interaction of Dfm1 and the Lipid Bilayer

The Rapoport lab recently demonstrated that Dfm1's homolog, Der1, forms a half channel with E3 ligase Hrd1 to induce lipid thinning, facilitating the retrotranslocation of ERAD-L substrates (20). To that end, we hypothesized that Dfm1 also retains membrane perturbation properties similar to Der1, enabling its removal of ERAD-M substrates. To investigate this, we collaborated with Rommie Amaro of UCSD to build a homology model of Dfm1 using the recently solved structure of Der1 as a template (20). Molecular Dynamics (MD) simulations were then performed, examining Dfm1's lipid interactions while embedded in a mixed lipid bilayer representative of the ER membrane. Lipid thickness in distant regions from Dfm1 was approximately 4.0-4.5 nm, expected for the phospholipid bilayer (42). Our MD simulations, however, observed rearrangement of lipids in the vicinity of Dfm1, near its TM1, TM2, and TM5 domains, both on the luminal and cytoplasmic side (Figure 11A-B). Lipid thinning was observed with a membrane thickness of approximately 2.0-2.5 nm (Figure 11C; *circled in blue*). Throughout the simulation, local lipid thinning remained in the same region, between TM2 and TM5 as well as between TM1 and TM2. The magnitude of this local lipid thinning was reported to occur in the same region as Der1 (22). Notably, the membrane thinning region between TM2 and TM5 is localized in an area that was also determined to be the lateral gate for bacterial rhomboid GlpG as well as yeast rhomboid Der1 (Figure 11A; *indicated with asterisk*) (22, 28, 43).

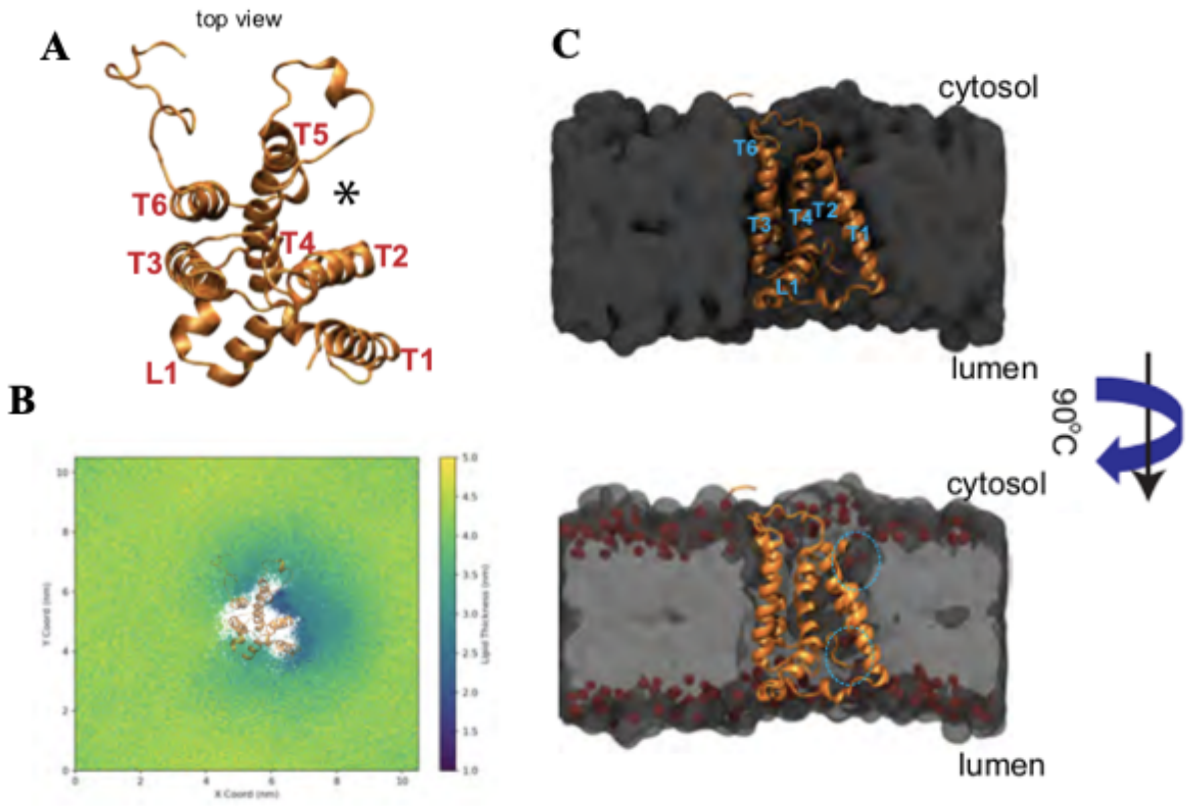

Figure 11. Dfm1 Interaction with the Lipid Bilayer
(A) Top view of *S. cerevisiae* derlin, Dfm1, homology mod el shown in gold ribbon with respective transmembrane domains and Loop 1 labeled. (B) Membrane thickness is shown as x and y 2D maps of the positions of the lipid head group every 1ns of simulation color-coded with the membrane thickness at that timepoint/location. The Dfm1 protein model is overlayed to show the relative locations of membrane thinning. Total thickness, i.e. the distance calculated between the upper and lower surfaces used for the analyses, is shown color-coded according to a 1.0 to 5.0 nm range. (C) Midpoint cross-section of the membrane where Dfm1 is embedded. Dfm1 is shown in gold ribbon, the lipids are shown in a grey volumetric representation, and the phospholipid head group is shown in red.

Dfm1 TM2 Mutants Disrupt Lipid Thinning Activity

The lipid deformation that was observed near TM1, TM2, and TM5 indicates a likely role for these transmembrane helices in lipid thinning and retrotranslocation activity for Dfm1. To analyze this region further, we performed MD simulations on TM residue mutant F107S from our random mutagenesis screen (previously validated for disrupting retrotranslocation but not disrupting substrate binding) and compared it to wildtype Dfm1 (Figure 12A-B). Simulations with

the F107S mutation in Dfm1 displayed lipid thinning in the vicinity of TM1 and TM2. While WT Dfm1 saw consistent thinning around TM1, TM2, and TM5, the F107S Dfm1 mutant saw a comparable thinning effect around TM2 and TM5 with a reduced thinning effect around TM1, at approximately 3.5-4.0 nm (Figure 12C). The mutant was also observed to significantly alter the structure of Dfm1, increasing the solvent accessible surface area (SASA) of the protein while having little to no effect on the total exposed surface area of the protein (Figure 12D). Thus, Dfm1 residue F107 appears to play a role in the structural stability of Dfm1. As observed, mutation of this residue affects Dfm1's lipid perturbing properties, rendering it completely dysfunctional in retrotranslocation (Figure 10E and Figure 12B).

Wu et al. reported that Dfm1's paralog, Der1, retains a hydrophilic stretch at TM2 (composed of residues NHLST) that are critical for its lipid thinning functions via their interactions with the lipid bilayer's phosphate head group (20). Dfm1 contains an analogous cluster of hydrophilic residues (RSSQ), where the Q101R retrotranslocation-deficient mutant from the screen is found. To test the potential role these hydrophilic TM2 residues play in Dfm1's function, we mutated these residues to hydrophobic amino acids, thus increasing TM2's hydrophobicity. Each mutant was found to reduce the degradation rate of Hmg2, with the strongest stabilization in the quadruple mutant: (R98L, S99V, S100V, and Q101L) (Figure 12E). Overall, this data suggests Dfm1 displays a mechanistic action of lipid thinning analogous to Der1.

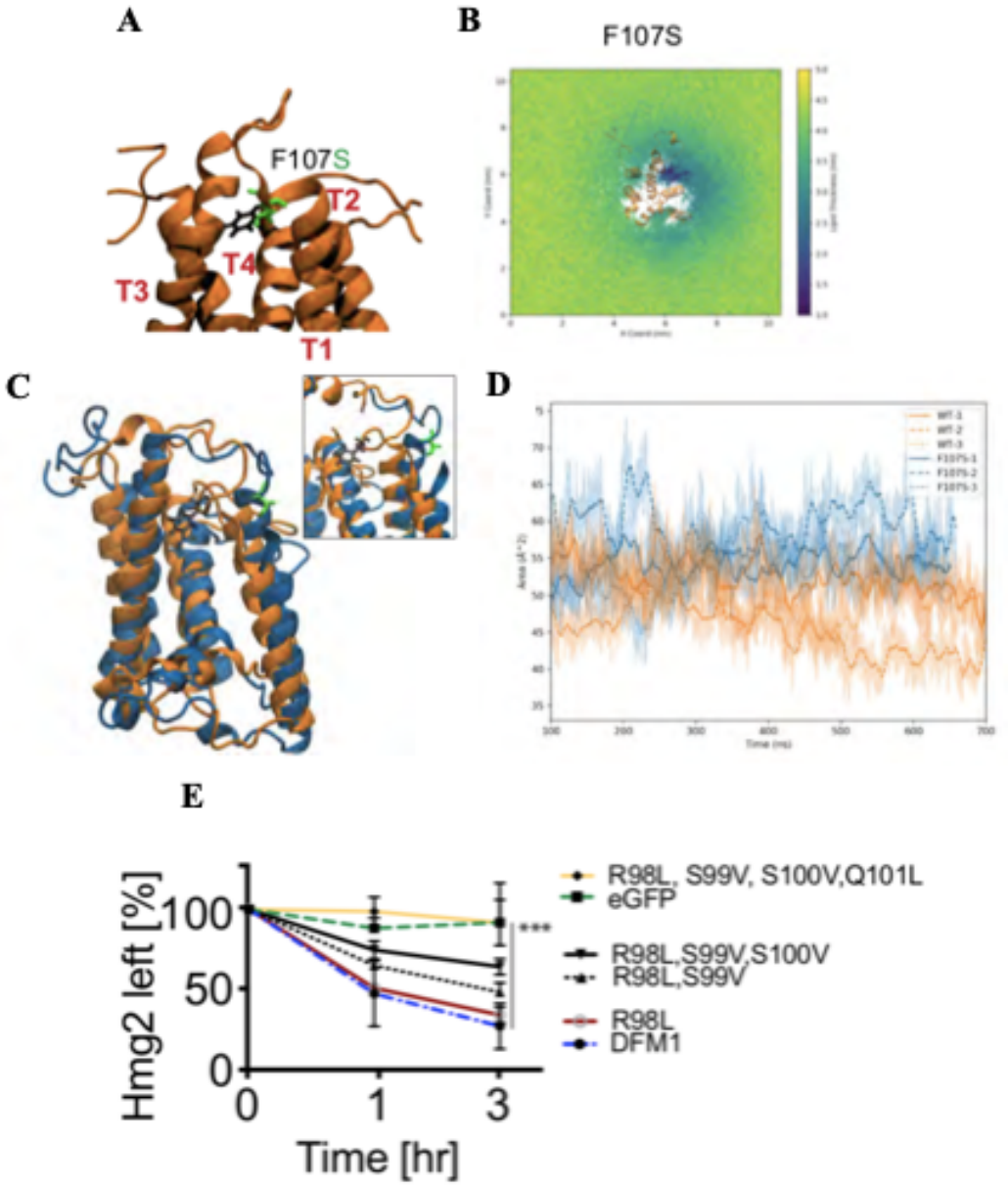

Figure 12. Dfm1 TM2 Mutants Disrupt Lipid Thinning Activity
(A) Homology model of Dfm1 with residues F107 shown in black and mutant residue F107S shown in green. (B) Same as (Fig. 11B) except membrane thickness was analyzed for Dfm1 mutant F107S. (C) Protein structure clusters with the highest prevalence (~50% of simulation time) of the WT protein (gold) and F107S protein (blue), highlighting the residue positional difference in F107 (black) and F107S (green). (D) SASA plots for the MD simulations with the shaded regions showing the raw data and the lines showing the 10 ns moving average. (E) *dfm1*Δ strains expressing the indicated Dfm1 mutants were grown to log-phase and degradation was measured by CHX-chase analysis. After CHX addition, Hmg2-GFP levels were measured by flow cytometry cells. Data is represented as mean ± SEM from at least three experiments, ***$p < 0.001$, Repeated Measures ANOVA.

Discussion

To provide valuable insights on the retrotranslocation function of rhomboid pseudoproteases and the mechanistic features of derlins, a subclass of rhomboid-like proteins widely represented in ER Associated Degradation, we investigated the structure of rhomboid derlin Dfm1. Specifically, we hypothesized that yeast Dfm1 retains key residues that pertain to its ability to move misfolded integral membrane substrates across the ER membrane in ERAD.

We discovered that residues in the Loop 1 and Transmembrane 2 regions of Dfm1 are critical for its actions. Closer analysis by another colleague in the Neal Lab revealed that the L1 retrotranslocation-deficient mutants were unable to detect membrane substrates, suggesting the residues in this region are essential for substrate binding. This result agrees with previous studies of bacterial rhomboid protease GlpG, where the L1 region in its structure was found to be significant for substrate binding (22). This raises the salient question: how does Loop 1 gain substrate access? One explanation is that Dfm1's L1 region attracts membrane substrates with unstable and/or positively charged transmembrane helices. Correspondingly, previous study of GlpG's structure has demonstrated that membrane substrates with helix breaking residues and restricted hydrophobicity readily move into GlpG's hydrophilic interior cavity (44). Another study on mammalian rhomboid protease RHBDL4 indicates it shows a preference of membrane substrates that have positively charged transmembrane helices (36). Another explanation may be that Dfm1's L1 region can aid in the diffusion of Dfm1 through the lipid bilayer, enabling it to inspect and identify membrane substrates that require retrotranslocation (24). Regardless of which answer may be true, understanding the mechanism of how Dfm1 detects and associates with substrates is of high significance, advancing the field of understanding regarding the rhomboid superfamily and protein quality control.

In order remove hydrophobic integral membrane proteins from their stable home within the lipid bilayer, Dfm1 (or really, any other protein with similar actions) must have a way of overcoming the great thermodynamic barrier in place (45). The unique structure of rhomboid proteins, including yeast derlins Dfm1 and Der1, has been proposed to reduce the thickness of the membrane bilayer, thus reducing the lipid permeability barrier, enabling the proteins to overcome the energetic barriers associated with retrotranslocation (11, 20, 22, 46). Using sequence analysis and molecular dynamics simulations of Dfm1's homology model, we were able to demonstrate that Dfm1 distorts its surrounding lipid bilayer. Furthermore, we identified a TM2 retrotranslocation-deficient mutant specifically disrupts lipid thinning in Dfm1.This result agrees with previous studies of both bacterial rhomboid GlpG as well as yeast derlin Der1, which was reported to induce lipid perturbation alongside E3 ligase Hrd1 to retrotranslocate luminal ERAD-L substrates (20, 43). Moreover, this kind of membrane perturbation exhibited by Der1 and Dfm1 lowers the energetic cost of removing membrane substrates (45). Since both Der1 and Dfm1 are rhomboid pseudoproteases that have retained the overall architecture of rhomboid proteases, with conserved residues to be found in both, this study yields potential information about other members of the rhomboid superfamily that may also work in the same way.

Overall, this study establishes that yeast derlin Dfm1 employs the unique features of the rhomboid superfamily, allowing it to carry out the widely conserved and critical process of membrane protein retrotranslocation. To test this out to some degree, Neal et al. chose to analyze Derlin-1, the closest human homolog to Dfm1, which shares more sequence similarity to Dfm1 than its yeast counterpart Der1 (41). Like Dfm1, Derlin-1 possesses a SHP tail to recruit p97/Cdc48 ATPase as well as the conserved WR and GxxxG motifs (18). They also found a subset of Dfm1 residues identified from the random mutagenesis and Alanine mutant screening

were also conserved in Derlin-1. To determine whether these conserved Derlin-1 residues were critical for ERAD, Neal et al. performed site-directed mutagenesis on these conserved residues and observed whether they were able to degrade Derlin-1's well-characterized multi-spanning membrane substrate, the clinically important disease causing mutant cystic fibrosis transmembrane conductance regulator *CFTRΔF508* using CHX-assays (46). In all cases, the normally degraded *CFTRΔF508* substrate was stabilized by all Derlin-1 mutants with levels similar to GFP only and WR mutant control. They also were able to determine that Derlin-1 L1 also contribute to membrane substrate binding of *CFTRΔF508*, indicating direct significance brought about by this study.

By and large, this study provides functional insight into derlin rhomboid pseudoproteases, ultimately serving future therapeutic design against rhomboid-like proteins associated with maladies ranging from cancer to neurological disorders.

Chapter 2, in full, has been submitted for publication of the material as it may appear in Molecular Cell, 2021. Nejatfard, Anahita; Neal, Sonya E; Wauer, Nicholas; Amaro, Rommie E. The thesis author was the primary author of this paper.

Chapter 3: Protein Purification Hindered by COVID19

Mammalian Rhomboids and their Physiological Role

Rhomboids are integral membrane proteins that are perhaps one of the most widely conserved protein families known and play a role in many diverse membrane-related processes (16). Rhomboids share a novel intramembrane serine protease activity that allows them to cleave substrate proteins in or near their transmembrane domains, subsequently releasing them from the membrane into the luminal or extracellular environments. Intramembrane proteases like rhomboids often catalyze the committed, signal-generating step of a variety of cell signaling pathways by cleaving transmembrane proteins within the membrane (31). It is this unique and highly preserved function of rhomboids, like many other intramembrane proteases, that leads to their implication in cancer, metabolic diseases, neurodegeneration, and more (32).

Significance of Mammalian Rhomboid Protease RHBDL4

Several intramembrane proteases have been linked to human pathologies such as neurodegeneration and cancer. For instance, the rhomboid-like protein PARL has been associated with Parkinson's (33) and type II diabetes (34). Another example is the inactivation of ERAD rhomboid RHBDL4 (otherwise known as RHBDD1) decreases tumor cell growth and has been shown to be associated with survival in patients with colorectal cancer (35). Further, RHBDL4 holds the capacity to cleave certain substrates localized in neurons, including the disease-causing mutant of the main adhesion molecule MPZ in the peripheral nervous system (36). It can also provide an alternative processing pathway for the amyloid precursor protein

family which are highly implicated in Alzheimer's Disease (21). Hence, studying RHBDL4's substrate specificity holds promise for deciphering the physiological role of RHBDL4.

RHBDL1 and RHBDL3 Substrate Profiling Remains a Mystery

To date, the physiological significance as well as the substrate selectivity of rhomboid proteases is unknown. Exciting preliminary data shows that active rhomboid protease, RHBDL1, is highly enriched in the stroma membrane of rat primary neurons (Figure 13). While an increasing number of substrates are being identified for rhomboids proteases such as PARL, RHBDL2, and RHBDL4, providing clues about their roles in health and disease, little is known about active rhomboid proteases, RHBDL1 and RHBDL3 (32). This is mainly due to the fact their substrates have yet to be identified. Despite retaining all the essential active site residues of related rhomboid proteins, they do not target RHBDL4/RHBDL2-associated substrates and likely possess their own substrate repertoire (32).

In fact, two different genetic screens have proposed the potential roles of RHBDL1 and RHBDL3. Organisms have evolved a specialized circadian system to adapt to environmental changes as day, night, and seasonal cycles change. Loss of synchrony between the internal circadian clock and these environmental light/dark changes is responsible for jet lag, and may also promote sleep disorders, metabolic disorders, and many other diseases (39). Utilizing high-throughput identification of genetic components by developing a machine-learning based algorithm, Zhang et al. were able to identify RHBDL1 knockout mice mutants as retaining impaired circadian misalignment behavior (38). The phenotype of homozygous knockout mice, however, was unable to be determined due to the mice displaying preweaning mortality or embryonic lethality. Further, heterozygous knockout mice showed altered glucose tolerance upon

survival and growth, which the authors found to suggest the deletion or haploinsufficiency of this gene impairs metabolism (38).

A separate genetic screen sought to identify a single gene or group of genes correlated with aging, preferentially those whose expression shows a linear relationship with age. Accordingly, Kumar et al. analyzed two large series of human brain samples for association of age and mRNA expression in the frontal cortex and cerebellum, using a single microarray platform by re-arraying previously collected samples. The gene with the most consistent and strongest association with aging, they found, was the expression of RHBDL3 (37). This finding, they suggested, might point to RHBDL3 as a valuable marker of aging, however further study is required before such a statement can be affirmed.

While both groups were unable to research the RHBDL1 and RHBDL3 genes further, the identification of these genes relevant to their studies point to poignant and important roles for these rhomboid proteases in mammalian adaptation and development, respectively.

Specific Goals and Aims

Our goal is to characterize the enzymatic activity of RHBDL1 and RHBDL3 in order to understand features of their substrates for selectivity. To achieve this goal, we aim to purify RHBDL1 and RHBDL3. To do this, we will clone both active and catalytically inactive versions of the mammalian rhomboids, transfecting them into expression HEK293-F cell lines. We will then solubilize both rhomboid proteases using the appropriate detergent for membrane proteins and purify them through both affinity chromatography and size exclusion chromatography. To our knowledge, we will be the first to fully purify and isolate these proteins. Our next aim is to biochemically validate RHBDL1/3-dependent substrates using the IQ Substrate Profiling Assay

established by Anthony O'Donoghue at UC San Diego. We are unsure of RHBDL1 and RHBDL3 bind to similar features with same proportions. One possibility is their spatial segregation is what confers substrate specificity. Another possibility is that they recognize completely different substrate features or motifs.

Once we have identified and validated substrates RHBDL1 and RHBDL3 target and cleave, we will understand the substrate features each rhomboid preferentially cleaves. This will aid in developing inhibitors specific to each rhomboid for future gene therapies and future characterization of a physiological role for these mammalian rhomboids.

My hypothesis is that mammalian rhomboids RHBDL1 and RHBDL3 each display their own different substrate selectivity.

* Unfortunately, this project began around the time the COVID-19 pandemic began, halting and subsequently decelerating the progress made in this project. I will thus be presenting the work to date*

Materials and Methods

Bacteria Growth Media

Escherichia coli Top10 cells were grown in standard LB media with ampicillin at 37°C. HEK293F cells were cultured in Freestyle 293 Media or Freestyle 293 Media supplemented with Opti-MEM.

Cloning

Plasmids used for this work were generated using standard molecular biology techniques and verified by sequencing (Eton Bioscience, Inc.). Full-length human RHBDL1 and RHBDL3 cDNA was obtained through Gibson cloning and PCR. Primers for this are listed in Table 5. The samples were then subcloned into pcDNA3.1/Myc-His(+)A (Invitrogen) to express RHBDL1/3 with the Myc-epitope and a 6xHis tag at the C-terminus.

Plasmid extractions consisted of transformants inoculated into 25mL LB+Kan media and grown overnight. The following day, the entire culture was pelleted and resuspended in 4 mL of resuspension buffer from the PureLink HiPure Plasmid DNA MidiPrep Kit (Invitrogen). The remainder of the Midiprep was carried out according to the manufacturer's protocol.

Table 5. List of Primers used for Cloning *RHBDL1* and *RHBDL3*

Plasmid	Primer	Sequence	Anneal T (°C)
RHBDL1	Forward	CTCTGGCTAACTAGAGAACCCACTGCTTAC TGGATCCGGTACCGAGGAGAT	67
	Reverse	CAGATCCTCTTCTGAGATGAGTTTCTGCTC	
RHBDL3	Forward	CTCTGGCTAACTAGAGAACCCACTGCTTAC GATCCGGTACCGAGGAGATCT	65
	Reverse	CAGATCCTCTTCTGAGATGAGTTTCTGCTC	

Site-Directed Mutagenesis

Plasmids used for this were generated using standard molecular biology techniques and verified by sequencing (Eton Bioscience, Inc.). Previously cloned RHBDL1/3 plasmids now expressing the Myc-epitope and 6xHis tag was amplified using Pfu UltraTaq Polymerase (New England BioLabs Inc.). Specifically, 200 ng of template DNA (RHBDL1 or RHBDL3) and 18 cycles of PCR were used to obtain 1 point mutation within the coding region. Primers used for this are listed in Table 6. Mutagenized catalytically inactive RHBDL1/3 was amplified with Pfu UltraTaq polymerase and treated with Dpn1 at 37°C for three hours to digest the original unmutagenized templated. The mutagenized plasmids were then transformed into chemically competent Top10 cells and selected on LB+Kanamycin plates and incubated at 30°C. Resulting colonies were colony purified. Colonies were recovered using Promega Wizard Plus SV Miniprep kit and sent to Eton for sequencing using primers from Table 5. Mutants containing one point mutation and no early stop codons verified by both forward and reverse strands were selected as mutants of interest.

Table 6. List of Primers used for DpnI Mediated Site-Directed Mutagenesis of *RHBDL1* and *RHBDL3*

Plasmid	Position	Mutation	Primer	Sequence	Anneal T (°C)
RHBDL1	312	S → A	Forward	CGGGCCCCGGTGGTGGGAGGC**gct**GGCGGGGTCTACGCCCTGTGC	68
			Reverse	GCACAGGGCGTAGACCCCGCC**agc**GCCTCCCACCACCGGGGCCCG	
RHBDL3	278	S → A	Forward	TGACCGCTCCAGTCGTGGGCTCT**gct**GGAGGGGTGTATGCTCTCGTC	68
			Reverse	GACGAGAGCATACACCCCTCC**agc**AGAGCCCACGACTGGAGCGGTCA	

Cell culture, Transfections, and Immunoblotting

HEK293F cell lines were cultured in Freestyle 293 Expression Medium (ThermoFisher) and grown at 37°C and 8% CO_2 in shaker flasks. Both pcDNA3.1-RHBDL1 and pcDNA3.1-RHBDL3 were co-transfected into HEK293F cells in a 1:1 ratio using FreestyleMax Reagent (ThermoFisher) according to the manufacturer's instructions. Ninety-six hours after transfection, cells were lysed in lysis buffer (150 mM NaCl, 50 mM Tris pH 8.0, 1% NP40, 0.1% SDS, and 0.5% sodium deoxycholate, supplemented with 1 mM EDTA and protease inhibitors) for thirty minutes on ice. After lysis, samples were resuspended in 2xLaemmeli loading buffer and subjected to immunoblotting analysis. Equal amounts of protein extracts were separated by SDS-PAGE, transferred on nitrocellulose membrane, and immunoblotted for anti-GAPDH (Bio-Rad) and anti-His (AbClonal Inc.).

DDM Solubilization

Plasmids were transfected into HEK293F cells and harvested after four days using cold PBS buffer. Cells were resuspended in minimal media lysis buffer (10 mM HEPES pH 8.0, 2 mM KCl, and Protease Inhibitors (PI)) and homogenized with 20 up and down strokes in a Dounce Homogenizer. Homogenate was centrifuged at 45,000 rpm for 30 minutes at 4°C. This step was performed two more times on the pellets. Pellet was then homogenized in minimal media lysis buffer supplemented with 1 M NaCl and 2 mM DTT and spun as before. Pellets were resuspended in solubilization buffer (50 mM HEPES pH 8.0, 500 mM NaCl, 10 mM Imidazole, and PIs) at a concentration of 40 mg/mL supplemented with 3.5% DDM and incubated for three hours. Lysate was clarified by centrifugation at 95,000 rpm for 1 hour at 4°C. Supernatant was then purified using nickel beads.

Batch Ni/NTA Purification

100 µL of nickel beads were used per mL of protein sample. Beads were washed in solubilization buffer twice, centrifuged at 700 x g for 2 minutes and aspirated. Protein samples were added to beads and incubated overnight at 4°C on nutator. The following day, beads were washed with solubilization buffer supplemented with 20 mM Imidazole, spun at 700 x g for 2 minutes, and aspirated. Protein samples were eluted from the beads using solubilization buffer supplemented with 300 mM Imidazole, incubated for 15 minutes at 4°C, and spun at 700 x g for 2 minutes (if following DDM, then wash and elution buffers were also supplemented with 0.1% DDM). Protein samples were then concentrated using Pierce Protein Concentrator tubes separated 10 kDa and above.

SMALPS Solubilization

Similar to DDM solubilization, except instead of adding 3.5% DDM to the solubilization buffer incubation, 3% SMA was added instead. Incubation, spin, and nickel purification followed as described.

Protein Concentrating

After eluting the protein from the Ni column, the eluate was centrifuged in 10 kDa Pierce Protein Concentrators PES (Thermo Fisher) at 2,500 x g at 4°C until the volume was concentrated to 1 mL. After confirming protein concentration using NanoDrop, the eluate was washed with a buffer comprised of 50 mM HEPES pH 8.0, 200 mM NaCl, 10% glycerol, and 0.1% DDM (if from the DDM Solubilization) to elute out the imidazole. Wash was spun at 2,500

x g at 4°C until volume was about 1 mL. Wash repeated once more. Protein aliquoted at flash frozen in liquid nitrogen. Stored at -80°C.

Bradford Reagent Assay

Bovine Serum Albumin (BSA) was prepared as a protein standard in buffer ranging from 0.1 mg/mL to 1.0 mg/mL. 1 mL of protein standard was prepared, and 1 mL of protein sample was prepared with 50 µL of purified protein added to 950 µL of buffer (used the protein concentrating buffer). 1 mL of Bradford Reagent was then added to standards and samples and incubated for 30 minutes. Absorbances were measured in UV Spec at 595 nm. Net absorbance vs. protein concentration of each sample was plotted using GraphPad Prism.

IQ-peptide-based Protease Kinetic Assay

The cleavage reaction mixture consisted of 100–200 µL of catalytically active protease (RHBDL1 or RHBDL3) mixed with 700-800 µL of buffer (20 mM citrate phosphate, 150 mM NaCl, 20% glycerol, 2 mM DTT, and 0.05% DDM for the DDM solubilized at pH 8.0). 15 µL of this was then combined with 15 µL of each respective IQ substrate. This was compared against both the catalytically inactive protease combined with buffer and substrates in the same way, as well as only the buffer combined with the substrates as a baseline control. Cleavage reactions were carried out over several time intervals with various amounts of enzyme and with substrate concentration at saturation level. The FRET based cleavage assay was conducted in a fluorescence multiwell plate reader (SynergyMx, BioTek, VT, USA). Upon excitation at 320 nm, the emission intensity at 400 nm was recorded at 3-min intervals for 2 hours and plotted with GraphPad PRISM software. The initial velocities were defined as the slopes of a graph of

generated product as a function of time. Catalytic parameters were extrapolated with GraphPad PRISM.

Results

Preliminary Data for RHBDL1 and RHBDL3

For many years, researchers have sought to identify potential roles for RHBDL1 and RHBDL3. Lemberg and Bergbold determined that both RHBDL1 and RHBDL3 retain structural signatures relevant to the rhomboid superfamily, including the WR motif in Loop1 and the GxxxG motif in TM6 (15). Localization studies appeared to indicate that RHBDL1 localizes to the Golgi while RHBDL3 localizes to endosomes. Ectopic expression of RHBDL1 and RHBDL3 was also seen to lead to partial colocalization with plasma membrane localized RHBDL2 substrates, several of which have been identified by candidate testing. However, no significant proteolytic activity was detected, suggesting the apparent lack of activity may be due to differences in substrate specificity.

In collaboration with the Patrick Lab of UCSD, the Neal Lab sought to map localization of RHBDL1. Mixed neuronal cultures from P1 Sprague Dawley rat pup hippocampi were processed for immunostaining at 15 DIV and blotted with primary antibodies RHBDL1 rabbit polyclonal and MAP2 chicken polyclonal for the control (Figure 13A). These immunofluorescence stains display expression of RHBDL1 in hippocampus neurons. Next, RHBDL1 was co-expressed in cortical neuron cultures and followed with immunoblotting using protein specific antibodies to measure expression throughout maturation (Figure 13B). When compared against controls, RHBDL1 showed strong expression levels throughout maturation (DIV 4-12) in primary cortical neuron cultures. This preliminary data implicates a potential role of RHBDL1 in neuronal function.

All this preliminary data advocates the need to identify the specific substrates associated with each rhomboid protein in order to characterize the potential roles and mechanisms they may undertake.

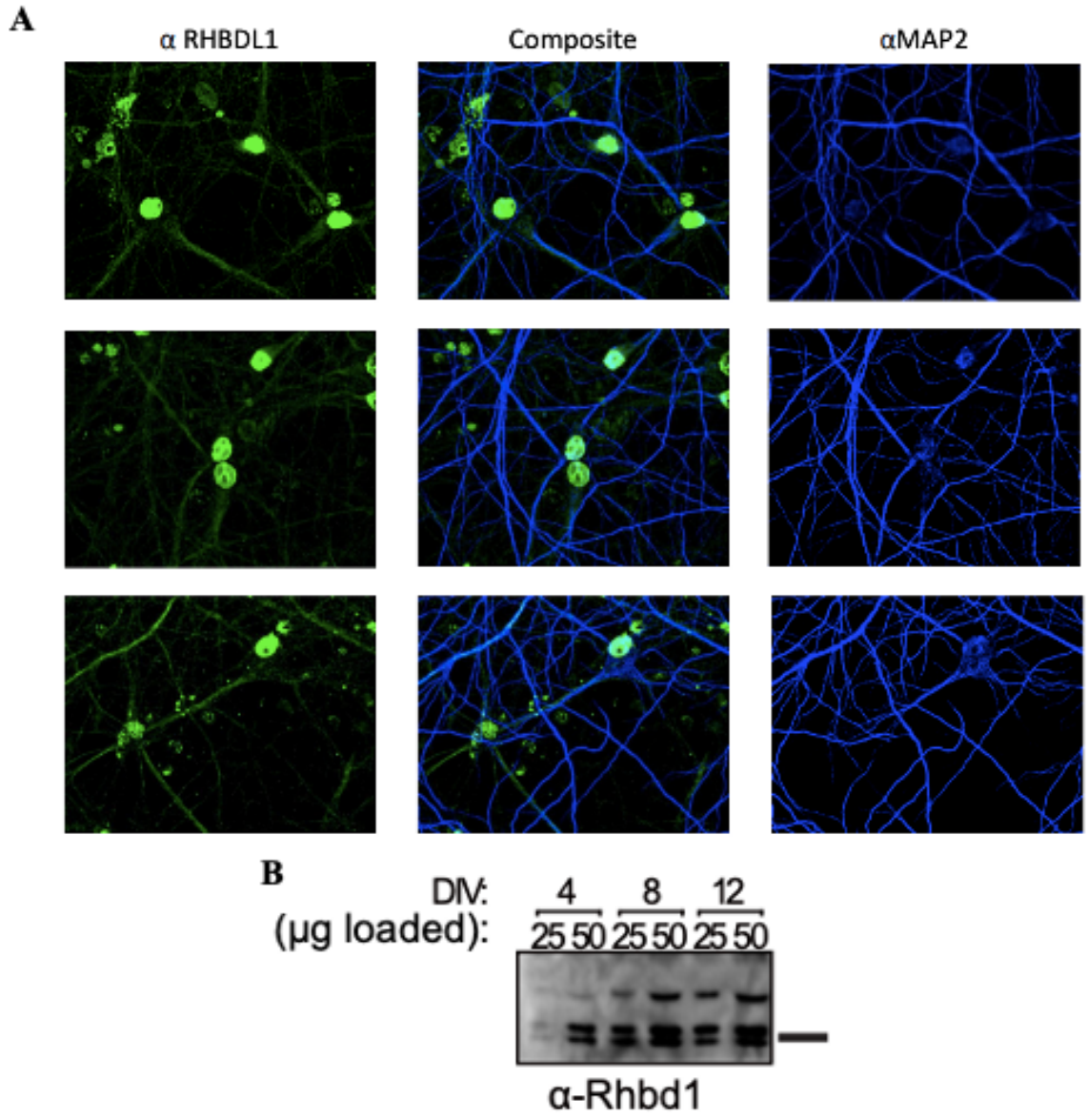

Figure 13. Preliminary Results of RHBDL1 Neuronal Culture
(A) RHBDL1 in hippocampus neurons. In collaboration with Gentry Patrick of UCSD, mixed neuronal cultures from P1 Sprague Dawley rat pup hippocampi were processed for immunostaining at 15 days in vitro (DIV) and blotted with primary antibodies RHBDL1 rabbit polyclonal and MAP2 chicken polyclonal for the control. (B) RHBDL1 shows strong expression levels through maturation in primary cortical neurons. RHBDL1 was co-expressed in cortical neuron cultures and followed with SDS-PAGE and immunoblotting using a-RHBDL1 primary antibody.

Transfection of RHBDL1 and RHBDL3

To perform any relevant studies on RHBDL1 and RHBDL3, both rhomboid proteins required cloning into a vector plasmid that would enable immunoblotting and later purification. Thus, the genes for RHBDL1 and RHBDL3 were amplified from mammalian CMV-RHBDL1(or 3)-Myc-Flag and transformed using homologous recombination into a -Myc-6xHis vector on their C-terminus. The Myc tag allows for immunoblotting with α-Myc antibody, and the His tag allows for both blotting with α-His antibody as well as later affinity column purification.

Additionally, catalytically inactive versions of each plasmid were also cloned through site-directed mutagenesis for future comparison. Both rhomboid proteins displayed the use of a catalytic histidine-serine dyad active site typical of proteases in the rhomboid superfamily (15). To develop catalytically inactive versions of the proteins, the catalytic serine at position 312 in RHBDL1 and at position 278 in RHBDL3 was mutated to an inactive alanine using DpnI-mediated Site-Directed Mutagenesis.

Both catalytically active and inactive versions of the mammalian rhomboids were then Midiprepped using the PureLink HiPure Midiprep Kit to concentrate the DNA for transfection. HEK293F cell lines were then cultured in Freestyle 293 Expression Medium and grown at 37°C and 8% CO2 in shaker flasks. Both RHBDL1 and RHBDL3 were co-transfected into 30 mL cultures of HEK293F cells containing thirty million cells in a 1:1 ratio of DNA to Freestyle Max Reagent. Two billion cells were harvested through centrifugation at 3,000 x g two-, four-, six-, and eight-days post-transfection and washed in ice cold PBS media. The cells were then lysed in lysis buffer and subjected to SDS-PAGE and immunoblotting for primary antibodies α-His and α-GAPDH for the control for validation (Figure 15A). Significant expression of both was detected, with a strong signal obtained by four days post-transfection. Future transfections would

be scaled to 90 mL cultures of ninety million cells and harvested in a similar manner for later solubilization and purification experiments.

DDM Solubilization of RHBDL1 and RHBDL3

Advances in structural biology are yielding an increasing number of membrane protein structures, however relatively few membrane protein structures have been determined in the presence of a lipid bilayer environment. Given that mammalian rhomboids are membrane proteases, it is important to isolate the proteins in a lipid-like environment to prevent disruption of structure of regions that could contribute to overall protein function. Typical membrane protein isolation studies are performed through solubilization of the membrane protein followed by purification using affinity or size exclusion chromatography.

The solubilization stage typically entails extraction of membrane proteins from their natural environment, the lipid membrane, to an aqueous environment using detergents. Detergents can disintegrate the lipid bilayer while incorporating lipids and proteins in detergent micelles. If successfully solubilized, the detergent micellar structures formed with the proteins and lipid allow for the hydrophilic parts of protein to remain in contact with the aqueous environment while the hydrophobic regions of the membrane protein and lipid tails are buried in the hydrophobic interior of the detergent micellar structure, enabling the protein to retain its active conformation (51).

Non-ionic detergent *n*-dodecyl-β-D-maltoside (DDM) has been considered a good starting detergent for membrane protein purification and has typically been the most successful (48). With its maltoside sugar headgroup and its twelve-carbon alkyl tail, DDM micelles have been shown to stabilize intact oligomeric membrane protein complexes. Its large size allows

better maintenance of a membrane protein in solution; however, it may also mean less of the protein is exposed to form protein-protein interactions (50). Prior to solubilizing with DDM, the membrane protein of interest must also be purified in a high ionic strength buffer to suppress heavy aggregation if the detergent is not necessarily optimal (50).

Accordingly, we solubilized our 30 mL protein harvests using DDM as our detergent for validation. To determine the proper incubation time, a three hour and four-hour solubilization was performed for both RHBDL1 and RHBDL3 with 3.5% DDM, with the lysate, supernatant, pellet, flowthrough, wash, and elution steps collected and analyzed by SDS-PAGE and immunoblotting with α-His antibody and α-GAPDH for control (Figure 15B). Both proteins are approximately 54 kDa in size: this band was confirmed on both blots. It appeared the three-hour solubilization eluted a significant amount of protein for both RHBDL1 and RHBDL3 solubilization; thus, we chose to proceed with three-hour DDM incubations for the proteins. Interestingly, both blots displayed several bands of varying sizes in addition to the expected 54 kDa band. While this can sometimes occur with membrane protein solubilization, the frequency of bands is notably different from what is expected (52).

Following DDM solubilization, the samples were purified using nickel bead affinity chromatography, which is highly selective for proteins containing an affinity tag of six consecutive Histidine residues. The samples were then concentrated using a 10 kDa protein concentrator, and snap frozen in liquid nitrogen. To assess the concentration of protein each sample contained, a Bradford Reagent Assay was also performed using bovine serum albumin (BSA) as the control standard (Figure 15D). All samples appeared to contain some concentration of protein and were thus ready to be assessed for substrate specificity.

IQ Substrate Assay of RHBDL1 and RHBDL3

To determine the substrate sequence specificity of RHBDL1 and RHBDL3, we chose to utilize the IQ Substrate Specificity Assay developed by the O'Donoghue lab of UCSD. Previously, O'Donoghue et al. utilized this assay to identify a soluble fluorescent substrate for activity assessment of three bacterial rhomboid proteases, GlpG from *E. coli* and *H. influenza* and PsAarA from *P. stuartii*, with seven commercially available internally quenched substrates (49). They were able to identify one substrate that was cleaved by all three rhomboid proteases; these enzymes were able to hydrolyze this substrate between amino acids norvaline and tryptophan (49).

In the same vein, we performed this assay by comparing the catalytically active versions of RHBDL1 and RHBDL3 against their catalytically inactive versions and a buffer baseline. The enzymes were assayed with a selection of internally quenched fluorescent substrates developed by the O'Donoghue lab to detect and biochemically characterize proteases in other organisms (Figure 14). A diverse library of peptides was generated by incorporated all combinations of neighbor and near-neighbor amino-acid pairs into decapeptide sequences flanked by unique dipeptides at each terminus (53). However, the results of our IQ assays showed no enzymatic activity for our proteases. In fact, the catalytically inactive versions of RHBDL1 and RHBDL3 appeared to show more activity than their catalytically active counterparts, indicating something was amiss with our DDM solubilization and purification experiments. Thus, we investigated another means of solubilizing the protein.

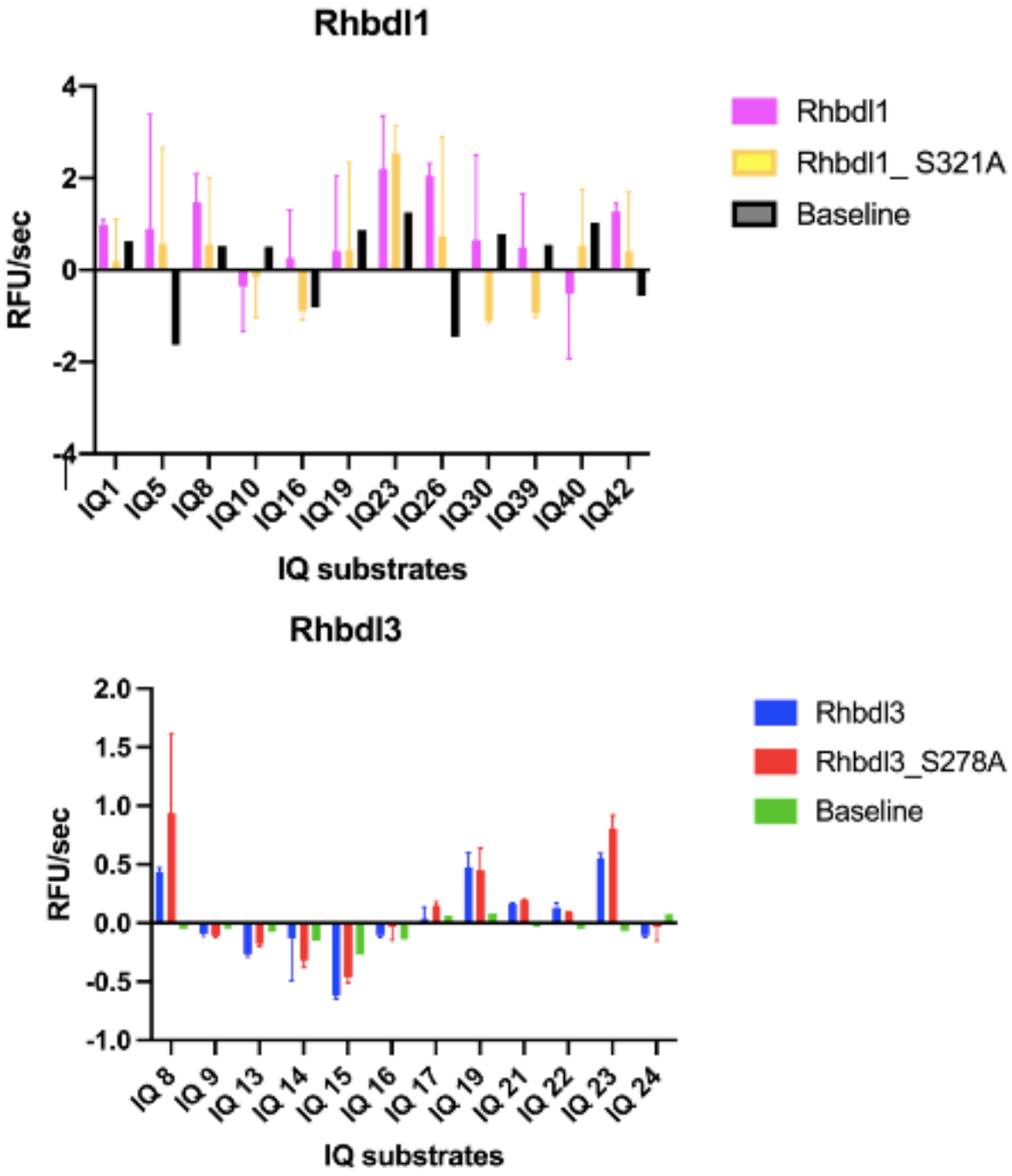

Figure 14. IQ Substrate Selectivity Assay on RHBDL1 and RHBDL3
IQ Substrate Specificity Assay of RHBDL1 and RHBDL3 against catalytically inactive versions and baseline buffer. Cleavage reaction combined 15 µL catalytically active (or inactive) protease with 15 µL individual IQ substrate. This was compared against baseline of 15 µL buffer mixed with 15 µL individual IQ substrate. Excitation occurred at 320 nm and emission intensity at 400 nm was recorded at 3-min intervals for 2 hours and plotted with GraphPad Prism.

SMA Solubilization of RHBDL1 and RHBDL3

A new approach to membrane protein extraction has been developed by utilizing a styrene-maleic acid (SMA) copolymer instead of conventional detergents. This polymer can insert itself into and cut up membranes, forming small discs of bilayer that are encircled by the polymer: this is known as SMALPs (SMA lipid particles) (47). Proteins encapsulated by SMALPs importantly do not form detergent micelles; instead, they hold the membrane protein in a lipid-like environment that mimics their native environment. It is a method that has successfully solubilized a number of membrane proteins (47). For this reason, we chose to utilize this method for solubilizing our mammalian rhomboid proteases.

Accordingly, we solubilized our 30 mL protein harvests of RHBDL1 and RHBDL3 using SMA nanodiscs using a protocol similar to the DDM solubilization. To determine the proper incubation time, a three hour and four-hour SMA solubilization was performed for both RHBDL1 and RHBDL3 with 3% SMA, with the lysate, supernatant, and pellet collected and analyzed by SDS-PAGE and immunoblotting with anti-His antibody and α-GAPDH for control (Figure 15C). In this blot, a single large faint band was able to be discerned in the pellets as well as the four hour incubated supernatants. If the rhomboid proteases are comprised of multiple subunits, then this single band likely indicates the multi-unit complex retained in the SMA lipid particle. Thus, we believed this solubilization could also work for the proteins.

However, upon attempting to scale up the solubilization to our 90 mL protein harvests, no protein was detected using the NanoDrop for neither RHBDL1 nor RHBDL3. Further, we could not concentrate the proteins like we were able to before with the DDM solubilization, indicating a need to optimize this protocol further. This lack of protein also prevented us from running the proteins through the IQ substrate specificity assay.

Figure 15. Transfection and Solubilization of Mammalian Rhomboids, RHBDL1 and RHBDL3
(A) Transfection validation of RHBDL1 and RHBDL3. $3x10^7$ total HEK293F cells were transfected in a 1:1 ratio of Freestyle Max Reagent to DNA. Four days post transfection, cells were harvested and lysed. Analysis was performed using SDS-PAGE and immunoblotted with primary antibodies α-His and α-GAPDH for control. (B) DDM Solubilization validation of RHBDL1 and RHBDL3. Harvested cells from (A) were solubilized with DDM according to protocol and purified using nickel bead affinity chromatography. Samples were collected at each stage of solubilization and purification, then analyzed using SDS-PAGE and immunoblotted with α-His and α-GAPDH for control. (C) Bradford Reagent Assay of Purified RHBDL1, RHBDL3, S312A, and S278A samples. BSA was used as a protein standard ranging from 0.1-1.0 mg/mL. Absorbances were measured in UV Spec at 595 nm. Net absorbance vs. protein concentration of each sample was plotted using GraphPad Prism. (D) SMA Solubilization Validation of RHBDL1 and RHBDL3. Similar protocol to (B) except solubilized with SMA. Lysate, supernatant, and pellet were analyzed using SDS-PAGE and immunoblotted with α-His and α-GAPDH for control prior to purification

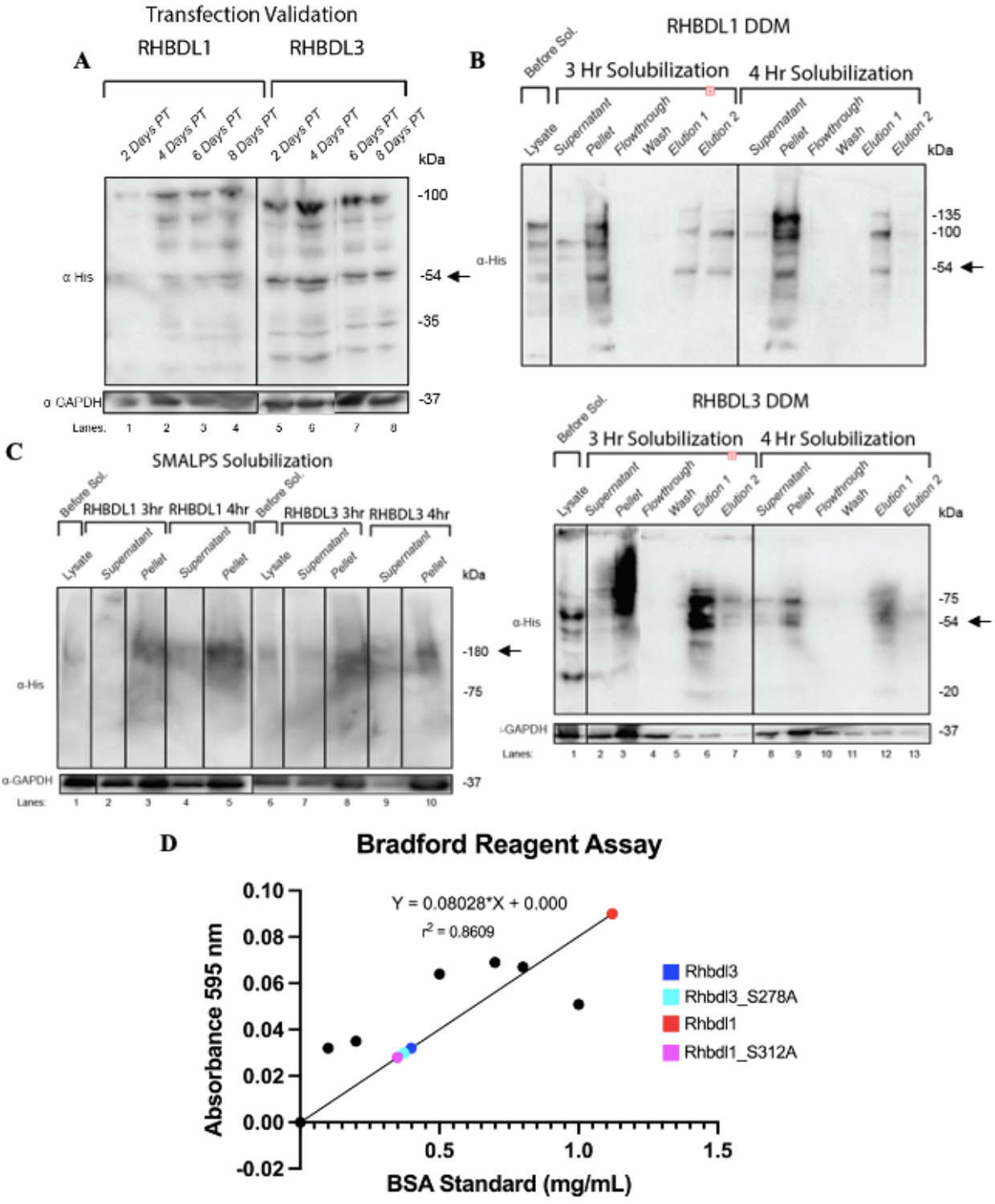
Transfection Validation
A
RHBDL1
RHBDL3
2 Days PT
4 Days PT
6 Days PT
8 Days PT
kDa
-100
-54
-35
-37
α His
α GAPDH
Lanes: 1 2 3 4 5 6 7 8
B
RHBDL1 DDM
Before Sol.
3 Hr Solubilization
4 Hr Solubilization
Lysate
Supernatant
Pellet
Flowthrough
Wash
Elution 1
Elution 2
-135
-100
-54
α-His
RHBDL3 DDM
-75
-20
-37
C
SMALPS Solubilization
RHBDL1 3hr
RHBDL1 4hr
RHBDL3 3hr
RHBDL3 4hr
-180
-75
α-GAPDH
Lanes: 1 2 3 4 5 6 7 8 9 10
D
Bradford Reagent Assay
Y = 0.08028*X + 0.000
r² = 0.8609
Absorbance 595 nm
0.10
0.08
0.06
0.04
0.02
0.00
-0.02
0.5
1.0
1.5
BSA Standard (mg/mL)
Rhbdl3
Rhbdl3_S278A
Rhbdl1
Rhbdl1_S312A

Discussion

Due to the rise of the COVID-19 pandemic, this project was seriously halted; however, our studies shed valuable insight on the potential structures of mammalian rhomboids RHBDL1 and RHBDL3. The structure-function relationship of rhomboid proteins and their relative substrate specificity are intriguing questions in the field. In this study, we attempted to purify RHBDL1 and RHBDL3 using two separate solubilization methods for later analysis using the IQ Substrate Specificity Assay. While we were unable to fully solubilize effective samples of RHBDL1 and RHBDL3 to perform the specificity assay, our solubilization studies provide valuable insight on how to purify those proteins.

n-dodecyl-β-D-maltoside (DDM) is typically a good starting detergent for membrane protein purification. While our attempts to solubilize and later purify RHBDL1 and RHBDL3 using this detergent yielded significant amounts of protein, the enzyme activity went undetected when attempting the IQ Assay. In fact, the catalytically inactive versions of RHBDL1 (S312A) and RHBDL3 (S278A) appeared to show more activity than their catalytically active counterparts. Given the incidence of multiple bands on our immunoblotted validation, we surmised three possibilities: one is that the proteins need further purification using size-exclusion column chromatography, in the event there are any impurities in the samples. However, this does not explain the lack of activity seen in the IQ assays. Another possibility is that the DDM solubilization was potentially too harsh for the proteins, resultantly leading to the denaturing of the proteins. Another possibility is that the mammalian rhomboid proteins are composed of multiple subunits and are getting separated into their respective units when using DDM as a detergent. This would explain the protein concentration detected from the Bradford Reagent Assay and prevents the proteins from displaying their enzymatic activity since their potential

subunits are unable to work together to identify substrate specificity. The latter two possibilities would also explain the presence of multiple bands on the analysis blots.

With this in mind, we chose to attempt solubilizing the membrane proteins using a styrene-maleic acid (SMA) copolymer instead of conventional detergents like DDM. The nature of this polymer would allow the membrane proteins to be held in an environment that mimics the lipid bilayer, thus holding the protein in its native conformation and enabling its activity. Thus, we solubilized our harvest rhomboid protein samples using 3% SMA. Our test blot on the incubated supernatant and pellet displayed a faint band, indicating the likely presence of the protein in the SMA lipid particle. However, attempting to scale up the solubilizations and follow with the Batch Ni/Nta Purification as before resulted in the total loss of our proteins. This lack of protein prevented analysis using the IQ substrate specificity assay. There may be a number of reasons for why the protein was lost. One possibility is that the amount of SMA was not sufficient to solubilize the proteins from the lipid membrane. Another possibility is that a longer incubation time was needed; given the faintness of the bands on the blot, this is a reasonable assumption. Another possibility is that the solubilized protein requires a different method of purification, however this is the least likely since it has been shown that SMALPs can be purified using affinity purification, specifically nickel affinity chromatography like what we used (47). A known limitation of using the SMALP nanoparticle is that the structure is sensitive to divalent cations and can chelate with them, inducing conformational change or strain that can cause too many of the maleic acid group to protrude from a single SMALP that causes the SMA to precipitate (47). Accordingly, more optimization is needed to determine why this solubilization did not work.

Despite the lack of significant progress made on this project due to the COVID-19 pandemic, the data we gathered provides unique insight into the process of purifying these mammalian rhomboid proteins. Further examination and investigation are needed to understand how to fully isolate these proteases in a way that retains their enzymatic activity.

References

1. Sun, Z, Brodsky, JL. Protein quality control in the secretory pathway. J of Cell Biol 2019; 10: 3171-3187.

2. Kandel, RR, Neal, SE. The role of rhomboid superfamily members in protein homeostasis: Mechanistic insight and physiological implications. BBA Mol Cell Res 2020; 1867: 118793.

3. Bhattacharya, A, Qi, L. ER-associated degradation in health and disease – from substrate to organism. J of Cell Sci 2019; 132.

4. Cho, JA, Chinnapen, DJF, Aamar, E, te Welscher, YM, Lencer, WI, Massol, R. Insights on the trafficking and retro-translocation of glycosphingolipid-binding bacterial toxins. Front Cell Infect Microbiol 2012; 2: 51.

5. Moon, HW, Han, HG, Jeon, YJ. Protein Quality Control in the Endoplasmic Reticulum and Cancer. Int J Mol Sci 2018; 19: 3020.

6. Hampton, RY, Garza, RM. Protein quality control as a strategy for cellular regulation: lessons from ubiquitin-mediated regulation of the sterol pathway. Chem Rev 2009; 109: 1561-1574.

7. Mehrtash, AB, Hochstrasser, M. Ubiquitin-dependent protein degradation at the endoplasmic reticulum and nuclear envelope. Semin Cell Dev Biol 2019b; 93: 111-124.

8. Vembar, SS, Brodsky, JL. One step at a time: endoplasmic reticulum-associated degradation. Nat Rev Mol Cell Biol 2008; 9:944-957.

9. Neal, SE, Syau, D, Nejatfard, A, Nadeau, S, Hampton, RY. HRD Complex Self-Remodeling Enables a Novel Route of Membrane Protein Retrotranslocation. iScience 2020; 23: 101493.

10. Hampton, RY, Sommer, T. Finding the will and the way of ERAD substrate retrotranslocation. Curr Opin Cell Biol 2012; 24: 460-6.

11. Neal, SE, Jaeger, PA, Duttke, S, Benner, C, Glass, C, Ideker, T, Hampton, RY. The Dfm1 derlin is required for ERAD retrotranslocation of integral membrane proteins. Mol Cell 2018; 69: 306-320.

12. Schmidt, CC, Vasic, V, Stein, A. Doa10 is a membrane protein retrotranslocase in er-associated protein degradation. Elife 2020; 9: 1-31.

13. Baldridge, RD, Rapoport, TA. Autoubiquitination of the Hrd1 Ligase Triggers Protein Retrotranslocation in ERAD. Cell 2016; 166: 394-407.

14. Garza, RM, Sato, BK, Hampton, RY. In vitro analysis of Hrd1p-mediated retrotranslocation of its multispanning membrane substrate 3-hydroxy-3-methylglutaryl (HMG)-CoA reductase. J Biol Chem 2009a; 284: 14710-14722.

15. Bergbold, N, Lemberg, MK. Emerging role of rhomboid family proteins in mammalian biology and disease. BBA Biomembranes 2013; 1828: 2840-2848.

16. Urban, S, Dickey, SW. The rhomboid protease family: a decade of progress on function and mechanism. Genome Biology 2011; 12: 231.

17. Lemberg, MK, Freeman, M. Functional and evolutionary implications of enhanced genomic analysis of rhomboid intramembrane proteases. Genome Res 2007; 17: 1634-1646.

18. Greenblatt, EJ, Olzmann, JA, Kopito, RR. Derlin-1 is a rhomboid pseudoprotease required for the dislocation of mutant α-1 antitrypsin from the endoplasmic reticulum. Nat Struct Mol Biol 2011; 18: 1147-1152.

19. Lilley, BN, Ploegh, HL. A membrane protein required for dislocation of misfolded proteins from the ER. Nature 2004; 429: 834-840.

20. Wu, X, Siggel, M, Ovchinnikov, S, Mi, W, Svetlov, V, Nudler, E, Liao, M, Hummer, G, Rapoport, TA. Structural basis of ER-associated protein degradation mediated by the Hrd1 ubiquitin ligase complex. Science 2020; 368: 1-13.

21. Paschkowsky, S, Hamze, M, Oestereich, F, Munter, LM. Alternative Processing of the Amyloid Precursor Protein Family by Rhomboid Protease RHBDl4. J Biol Chem 2016; 291: 21903-21912.

22. Bondar, AN, del Val, C, White, SH. Rhomboid Protease Dynamics and Lipid Interactions. Structure 2009; 17: 395-405.

23. Tsai, YC, Weissman, AM. A ubiquitin-binding rhomboid protease aimed at ERADication. Dev Cell 2012; 23: 454-6.

24. Kreutzberger, AJB, Ji, M, Aaron, J, Mihaljevic, L, Urban, S. Rhomboid distorts lipids to break the viscosity-imposed speed limit of membrane diffusion. Science 2019; 363.

25. Eftekharzadeh, B, Hyman, BT, Wegmann, S. Structural studies on the mechanism of protein aggregation in age related neurodegenerative diseases. Mech Ageing Dev 2016; 156: 1-13.

26. Gardner, RG, Swarbrick, GM, Bays, NW, Cronin, SR, Wilhovsky, S, Seelig, L, Kim, C, Hampton, RY. Endoplasmic Reticulum Degradation Requires Lumen to Cytosol Signaling: Transmembrane Control of Hrd1p by Hrd3p. J Cell Biol 2000; 151: 69-82.

27. Brooks, CL, Lemieux, MJ. Untangling structure-function relationships in the rhomboid family of intramembrane proteases. BBA Biomembranes 2013; 1828: 2862-2872.

28. Wang, Y, Zhang, Y, Ha, Y. Crystal structure of a rhomboid family intramembrane protease. Nature 2006; 444: 179-80.

29. Kelley, LA, Mezulis, S, Yates, CM, Wass, MN, Sternberg, MJE. The Phyre2 web portal for protein modelling, prediction and analysis. Nat Protoc 2015; 10: 845-858.

30. Flagg, MP, Kao, A, Hampton, RY. Integrating after CEN Excision (ICE) Plasmids: Combining the ease of yeast recombination cloning with the stability of genomic integration. Yeast 2019; 36: 593-605.

31. Baker, RP, Urban, S. Cytosolic extensions directly regulate a rhomboid protease by modulating substrate gating. Nature 2015; 523: 101-105.

32. Dusterhoft, S, Kunzel, U, Freeman, M. Rhomboid proteases in human diseases: Mechanisms and future prospects. BBA Mol Cell Res 2017; 1864: 2200-2209.

33. Shi, G, Lee, JR, Grimes, DA, Racacho, L, Ye, D, Yang, H, Ross, OA, Farrer, M, McQuibban, GA, Bulman, DE. Functional alteration of PARL contributes to mitochondrial dysregulation in Parkinson's disease. Hum Mol Genet 2011; 20: 1966-74.

34. Walder, K, Kerr-Bayles, L, Civitarese, A, Jowett, J, Curran, J, Elliot, K, Trevaskis, J, Bishara, N, Zimmet, P, Mandarino, L, Ravussin, E, Blangero, J, Kissebah, A, Collier, GR. The mitochondrial rhomboid protease PSARL is a new candidate gene for type 2 diabetes. Diabetologia 2005; 48: 459-68.

35. Song, W, Liu, W, Zhao, H, Li, S, Guan, X, Ying, J, Zhang, Y, Miao, F, Zhang, M, Ren, X, Li, X, Wu, F, Zhao, Y, Tian, Y, Wu, W, Fu, J, Liang, J, Wu, W, Liu, C, Yu, J, Zong, S, Miao, S, Zhang, X, Wang, L. Rhomboid domain containing 1 promotes colorectal cancer growth through activation of the EGFR signaling pathway. Nat Commun 2015; 24: 8022.

36. Fleig, L, Bergbold, N, Sahasrabudhe, P, Geiger, B, Kaltak, L, Lemberg, MK. Ubiquitin-dependent intramembrane rhomboid protease promotes EAD of membrane proteins. Mol Cell 2012; 47: 558-69.

37. Kumar, A, Gibbs, JR, Beilina, A, Dillman, A, Kumaran, R, Trabzuni, D, Ryten, M, Walker, R, Smith, C, Traynor, BJ, Hardy, J, Singleton, AB, Cookson, MR. Age associated changes in gene expression in human brain and isolated neurons. Neurobiol Aging 2013; 34: 1199-1209.

38. Zhang, T, Xie, P, Dong, Y, Liu, Z, Zhou, F, Pan, D, Huang, Z, Zhai, Q, Gu, Y, Wu, Q, Tanaka, N, Obata, Y, Bradley, A, Lelliott, CJ, Nutter, LMJ, McKerlie, C, Flenniken, AM, Champy, MF, Sorg, T, Herault, Y, De Angelis, MH, Durner, VG, Mallon, AM, Brown, SDM, Meehan, T, Parkinson, HE, Smedley, D, Lloyd, KCK, Yan, J, Gao, X, Seong, JK, Wang, CKL, Sedlacek, R, Liu, Y, Rozman, J, Yang, L, Xu, Y. High-throughput discovery of genetic determinants of circadian misalignment PLoS Genet 2020; 16.

39. Roenneberg, T, Merrow, M. The Circadian Clock and Human Health. Curr Biol 2016; 26: R432-43.

40. Goder, V, Carvalho, P, Rapoport, TA. The ER-associated degradation component Der1p and its homolog Dfm1p are contained in complexes with distinct cofactors of the ATPase Cdc48p. FEBS Lett 2008; 582: 1575-1580.

41. Sato, BK, Hampton, RY. Yeast Derlin Dfm1 interacts with Cdc48 and fucntions in ER homeostasis. Yeast 2006; 23: 1053-1064.

42. Bondar, AN. Phosphatidylglycerol Lipid Binding at the Active Site of an Intramembrane Protease. J Membr Biol 2020; 253: 563-576.

43. Lemieux, MJ, Fischer, SJ, Cherney, MM, Bateman, KS, James, MNG. The crystal structure of the rhomboid peptidase from Haemophilus influenzae provides insight into intramembrane proteolysis. Proc Natl Acad Sci USA 2007; 104: 750-754.

44. Moin, SM, Urban, S. Membrane immersion allows rhomboid proteases to achieve specificity by reading transmembrane segment dynamics. Elife 2012; 1.

45. Marinko, JT, Huang, H, Penn, WD, Capra, JA, Schlebach, JP, Sanders, CR. Folding and Misfolding of Human Membrane Proteins in Health and Disease: From Single Molecules to Cellular Proteostasis. Chem Rev 2019; 119: 5537-5606.

46. Sun, F, Zhang, R, Gong, X, Geng, X, Drain, PF, Frizzell, RA. Derlin-1 promotes the efficient degradation of the cystic fibrosis transmembrane conductance regulator (CFTR) and CFTR folding mutants. J Biol Chem 2006; 281: 36856-36863.

47. Pollock, NL, Lee, SC, Patel, JH, Gulamhussein, AA, Rothnie, AJ. Structure and function of membrane proteins encapsulated in a polymer bound lipid bilayer. BBA Biomembranes 2018; 1860: 809-817.

48. Rouse, SL, Marcoux, J, Robinson, CV, Sansom, MSP. Dodecyl Maltoside Protects Membrane Proteins in Vacuo. Biophys J 2013; 105: 648-656.

49. Arutyunova, E, Jiang, Z, Yang, J, Kulepa, AN, Young, HS, Verhelst, S, O'Donoghue, AJ, Lemieux, MJ. An internally quenched peptide as a new model substrate for rhomboid intramembrane proteases. Biol Chem 2018; 399: 1389-1397.

50. Gutmann, DAP, Mizohata, E, Newstead, S, Ferrandon, S, Postis, V, Xia, X, Henderson, PJF, van Veen, HW, Byrne, B. A high-throughput method for membrane protein solubility screening: the ultracentrifugation dispersity sedimentation assay. Protein Sci 2007; 16: 1422-1428.

51. Lichtenberg, D, Ahyayauch, H, Goni, FM. The Mechanism of Detergent Solubilization of Lipid Bilayers. Biophys J 2013; 105: 289-299.

52. Lantez, V, Nikolaidis, I, Rechenmann, M, Vernet, T, Noirclerc-Savoye, M. Rapid automated detergent screening for the solubilization and purification of membrane proteins and complexes. Eng Life Sci 2015; 15: 39-50.

53. O, Donoghue, AJ, Eroy-Reveles, AA, Knudsen, GM, Ingram, J, Zhou, M, Statnekov, JB, Greninger, AL, Hostetter, DR, Qu, G, Maltby, DA, Anderson, MO, DeRisi, JL, McKerrow, JH, Burlingame, AL, Craik, CS. Global Identification of Peptidase Specificity by Multiplex Substrate Profiling. Nat Methods 2012; 9: 1095-1100.